

Plasmarings as dual black rings

Subhaneil Lahiri^(a,b) and Shiraz Minwalla^(a)

^(a)*Department of Theoretical Physics, Tata Institute of Fundamental Research,
Homi Bhabha Rd, Mumbai 400005, India*

^(b)*Jefferson Physical Laboratory, Harvard University, Cambridge MA 02138, USA*

November 7, 2018

Abstract

We construct solutions to the relativistic Navier-Stokes equations that describe the long wavelength collective dynamics of the deconfined plasma phase of $\mathcal{N} = 4$ Yang Mills theory compactified down to $d = 3$ on a Scherk-Schwarz circle and higher dimensional generalisations. Our solutions are stationary, axially symmetric spinning balls and rings of plasma. These solutions, which are dual to (yet to be constructed) rotating black holes and black rings in Scherk-Schwarz compactified AdS_5 and AdS_6 , and have properties that are qualitatively similar to those of black holes and black rings in flat five dimensional supergravity.

Contents

1	Introduction	2
2	Fluid mechanics and thermodynamics	7
2.1	Perfect fluid stress tensor	8
2.2	Dissipative part	8
2.3	Surface contribution	8
2.4	Equations of state	9
3	Rigidly rotating configurations	10
3.1	Equations of motion	11
3.2	Spinning ball	12
3.3	Spinning ring	13

4	Thermodynamic Potentials	14
4.1	Densities	14
4.2	Integrals	15
4.2.1	Spinning ball	15
4.2.2	Spinning ring	15
4.3	Temperature and angular velocity	15
5	Solutions at fixed energy and angular momentum	16
5.1	Existence	16
5.2	Validity	18
5.3	Global stability and phase diagram	20
5.4	Comparison with black rings in flat 5D space	20
5.5	Turning point stability	23
6	Four dimensional plasmarings	25
6.1	Stress tensor and equations of motion	26
6.2	Solutions	27
6.2.1	Ordinary ball	30
6.2.2	Pinched ball	30
6.2.3	Ring	31
6.2.4	Hollow ball	32
6.2.5	Hollow ring and toroidally hollowed ball	32
7	Discussion	34
A	Five dimensional plasmarings	36
B	Notation	38

1 Introduction

A particularly interesting entry in the dictionary between gauge theory and gravity links deconfined or ‘gluon plasma’ phase of Yang Mills theory to black branes and black holes in gravity. In this paper we study aspects of this connection in the context of specific examples. In most of this paper we study $d = 4$, $SU(N)$, $\mathcal{N} = 4$ Yang-Mills at ’t Hooft coupling $g_{YM}^2 N = \lambda$, compactified on a Scherk-Schwarz S^1 (the remaining $2 + 1$ dimensions are non compact). The low energy dynamics of this theory is that of a $2 + 1$ dimensional Yang-Mills system that undergoes deconfining phase transition at a finite temperature [1]. At large N and strong ’t Hooft coupling this system admits supergravity dual description; the low temperature confining phase is dual to a gas of IIB supergravitons on the so called AdS soliton background [1]

$$ds^2 = L^2 \alpha' \left(e^{2u} (-dt^2 + T_{2\pi}(u) d\theta^2 + dw_i^2) + \frac{1}{T_{2\pi}(u)} du^2 \right), \quad (1)$$

where $i = 1, \dots, 2$, $\theta \sim \theta + 2\pi$, $L^2 = \sqrt{\lambda}$ and¹

$$T_x(u) = 1 - \left(\frac{x}{\pi} e^u\right)^{-4}. \quad (2)$$

The high temperature phase of the same system (at temperature $\mathcal{T} = 1/\beta$) is dual to the black brane

$$ds^2 = L^2 \alpha' \left(e^{2u} (-T_\beta(u) dt^2 + d\theta^2 + dw_i^2) + \frac{1}{T_\beta(u)} du^2 \right). \quad (3)$$

The thermodynamics of the high temperature phase are determined in the bulk description by the usual constitutive equations of black brane thermodynamics [2]

$$P = -f = \frac{\pi^2 N^2}{8\mathcal{T}_c} (\mathcal{T}^4 - \mathcal{T}_c^4). \quad (4)$$

For $\mathcal{T} > \mathcal{T}_c$ this free energy is negative, and so (in the large N limit) is smaller than the $\mathcal{O}(1)$ free energy of the ‘confined’ gas of gravitons. Consequently, the system undergoes a deconfinement phase transition at temperature \mathcal{T}_c .²

Just as the mean equilibrium properties of the deconfined phase are well described by the equations of thermodynamics, the statistically averaged near-equilibrium dynamics of this phase is governed by the equations of fluid dynamics - the relativistic generalisation of the Navier-Stokes equations. These equations accurately describe the time evolution of fluid configurations whose space time derivatives are all small in units of the mean free path, which is of the same order as the mass gap of the theory [2,3]. The same equations, augmented by appropriate surface terms, may also be used to study the dynamics of large lumps of plasma localised in the gauge theory vacuum.

The properties of the surface that separates the plasma from the vacuum, may be studied in the context of the simplest plasma profile with a surface; a configuration in which half of space, $x < 0$, is filled with the plasma. The surface at $x = 0$ is a domain wall that separates the plasma from the vacuum. The net force on this domain wall vanishes (and so the system is in equilibrium) when the plasma that fills $x < 0$ has vanishing pressure, i.e. at $\mathcal{T} = \mathcal{T}_c$ in the large N limit. The bulk gravity dual of this solution was constructed numerically in [2]; this configuration interpolates between the black brane at $\mathcal{T} = \mathcal{T}_c$ for $x < 0$ and the vacuum at $x > 0$, via a domain wall. The thickness and surface tension of this domain wall may be read off from this gravitational solutions, and were estimated, in [2] at approximately $6 \times \frac{1}{2\pi\mathcal{T}_c}$ and $\sigma = 2.0 \times \frac{\pi^2 N^2 \mathcal{T}_c^2}{2}$.

More generally, one would expect a finite lump of plasma that evolves according to the relativistic Navier-Stokes equations map in the bulk to a ‘black hole’ that evolves according to the Einstein equations. Provided all length scales in the plasma solution are

¹Notice that, at large u , $T_x(u) \simeq 1$, so (1) reduces to AdS_{d+2} in Poincaré-patch coordinates, with u as the radial scale coordinate, and with one of the spatial boundary coordinates, θ , compactified on a circle (the remaining boundary coordinates, w_i and t , remain non-compact).

² $\mathcal{T}_c = 1/2\pi$ in the dimensionless units of (3)

small compared to the gauge theory mass gap (which is of the same order as the domain wall thickness), the dual bulk solution is well approximated by a superposition of patches of the black brane solution (with temperature varying across the patches) in the bulk and patches of the domain wall solution described in the previous paragraph. It follows (at least for stationary solutions) that the 3 dimensional black hole horizon topology (at any given time) is given by an S^1 (physically this is the θ circle) fibred over the two dimensional fluid configuration at the same time, subject to the condition that the S^1 contracts at all fluid boundaries. Consequently, fluid configurations with different topologies yield bulk dual black hole configurations with distinct horizon topologies. We will return to this point below.

This paper is devoted to a detailed study of certain ‘stationary’ configurations of the plasma fluid; i.e. time independent, steady state solutions to the relativistic Navier-Stokes equations. The simplest configurations of this sort was studied already in [2]; the plasmaball is a static, spherically symmetric lump of fluid at constant local pressure P with $P = \sigma/R$ where R is the radius of the lump and σ its surface tension. In this paper we study the more intricate spinning lumps of stationary fluid. These lumps carry angular momentum in addition to their mass.

It turns out that the relativistic Navier-Stokes equations admit two distinct classes of solutions of these sort. The first class of solution is a simple deformation of the static plasmaball; it is given by plasmaballs that spin at a constant angular velocity. The centripetal force needed to keep the configuration rotating in this solution is provided by a pressure gradient. The local plasma pressure (and hence local temperature and density) decreases from the edge (where it is a positive number set by the radius, surface tension and rotation speed) to the centre. As large enough angular velocity the pressure goes sufficiently negative in the core of the solution to allow for a second kind of solution of these equations; an annulus of plasma fluid rotating at constant angular velocity ω . The local plasma pressure is positive on the outer surface and negative at the inner surface; the numerical value of the pressure in each case precisely balances the surface tensions at these boundaries.

We now describe the moduli space of spinning plasmaball and plasma ring solutions in a little more detail. In fig.1(a) we have plotted the energy-angular momentum plane, which we have divided up into 4 regions. In region \hat{C} (low angular momentum at fixed energy) the only rigidly rotating solution to the equations of fluid dynamics is the rotating plasmaball. At higher angular momentum (region \hat{B}) in addition to the rotating plasmaball there exist two new annulus type solutions which we call large and small ring solutions. As their names makes clear, the solutions are distinguished by their size; the large ring has a larger outer radius than the small one. On further raising angular momentum (region \hat{A}), the small ring and the ball cease to exist; in this region the large ring is the only solution. Finally, at still larger angular momentum (region \hat{O}) there exist no solutions.

In fig.1(b) we have plotted the entropy of the three different kinds of solutions as a function of their angular momentum at a particular fixed energy. At angular momenta for which all three solutions coexist (region \hat{B}) the entropy of the small ring is always smaller than the entropy of either the large ring or the black hole. Upon raising the angular momentum, the solution with dominant entropy switches from being the ball to the large

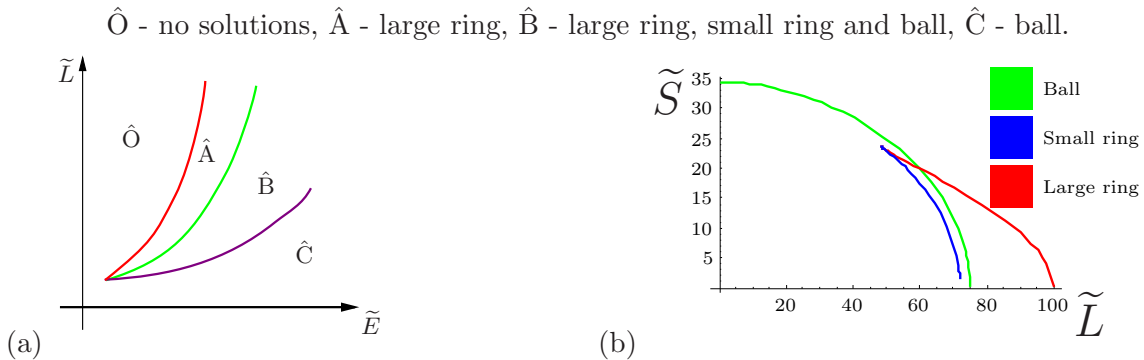


Figure 1: (a) Regions where ball and ring solutions exist, (b) their entropy as a function of angular momentum at fixed energy.

ring; the first order transition between these solutions occurs at an angular momentum that lies on a ‘phase transition line’ in the bulk of region \hat{B} . This picture suggests - and we conjecture - that the ball and the large ring are locally stable with respect to axisymmetric fluctuations, while the small ring is locally unstable to such fluctuations.³ In §5.5 we perform a ‘turning point’ analysis of our solutions, to find some evidence for this guess.

Let us now turn to the bulk dual interpretation of our solutions. The fluid for the spinning plasmaball is topologically a disk; consequently the horizon topology for the dual bulk solution - the S^1 fibration over this disk - yields an S^3 . The bulk dual of the spinning plasmaball is simply a rotating five dimensional black hole. On the other hand the fluid configuration of the plasmaring has the topology of $S^1 \times \text{interval}$; the S^1 fibration over this configuration yields $S^1 \times S^2$; i.e. a five dimensional black ring! Notice that in addition to the isometry along the S^1 , these ring solutions all have a isometry on the S^2 corresponding to translations along the Scherk-Schwarz circle. This additional isometry, that does not appear to be required by symmetry considerations, appears to be a feature of all known black ring solutions in flat space as well.

Using the gauge theory / gravity duality, the quantitative versions of the fig.1 give precise quantitative predictions for the existence, thermodynamic properties and stability of sufficiently big black holes and black rings in Scherk-Schwarz compactified AdS_5 spaces. While these gravitational solutions have not yet been constructed, their analogues in flat 5 dimensional space are known, and have been well studied. The general qualitative features (and some quantitative features) of fig.1 are in remarkably good agreement with the analogous plots for black holes and black rings in flat five dimensional space (see §5.4 for a detailed discussion).

The constructions we have described above admit simple generalisations to plasma solutions dual to black holes and black rings in Scherk-Schwarz compactified AdS_6 space.⁴

³It is possible that the large ring exhibits Plateau-Rayleigh type instabilities that break rotational invariance; such modes would map to Gregory-Laflamme type instabilities of the bulk solution (see also [4]). We thank T. Wiseman for suggesting this possibility.

⁴Note that the spinning plasmaring has no analogue in 1+1 dimensional fluid dynamics, for the excellent

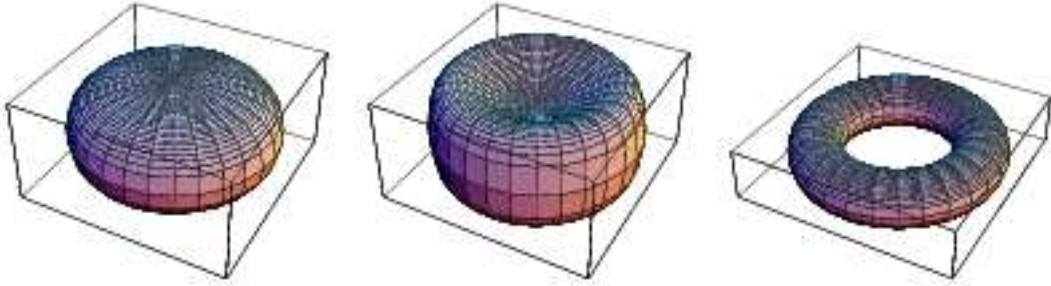


Figure 2: Spinning ball and ring solutions.

As the qualitative nature of the moduli space of black hole like solutions in six dimensional gravity is poorly understood, this study is of interest. The boundary duals of these objects, in the long wavelength limit, are stationary solutions to the equations of fluid dynamics of a 4 dimensional field theory. In §6 we construct such solutions. It turns out that these solutions occur in two qualitatively distinct classes. The simplest solutions are simply spinning balls of plasma; the fact that these balls spin causes them to flatten out near the ‘poles’. As these balls are spun up, their profile begins to ‘dip’ near the poles (see fig.2). As these balls are further spun up, they pinch off at the centre and turn into doughnut shaped rings (see fig.2).

As in the three dimensional case, the horizon topology of the black objects dual to the rotating plasmaballs and plasmaring described above, is obtained by fibering the fluid configuration with an S^1 that shrinks to zero at the fluid edges. This procedure yields a horizon topology S^4 for the dual to the rotating plasmaball, and topology $S^3 \times S^1$ for the dual to the plasmaring. As plasmaball and plasmaring configurations appear to exhaust the set of stationary fluid solutions to the equations of fluid dynamics, it follows that arbitrarily large stationary black objects in Scherk-Schwarz compactified AdS_6 all have one of these two horizon topologies. $S^2 \times S^2$ is an example of another topology one could have imagined for black objects in this space; these would have been dual to hollow shells of rotating fluid; however, there are no such stationary solutions to the equations of fluid dynamics.

The analysis of four dimensional fluid configurations, described above, demonstrates the power of the fluid dynamical method. In simple contexts, the Navier-Stokes equations are much easier to solve than the full set of Einstein’s equations, and rather easily reveal interesting and nontrivial information. It would be interesting to extend our analysis of fluid dynamical models in various directions to obtain information about the moduli space and stability of classes of black solutions in AdS spaces. An obvious extension would be to move to higher dimensions. As a first step in this direction, we have obtained and partially solved the fluid flow equations in 5 dimensional spaces. A complete analysis of

reason that there is no spin. This tallies with the fact that there are no black rings in four dimensions (at least in flat space).

these equations would yield the spectrum of black holes in Scherk-Schwarz compactified AdS₇ spaces, in terms of the fluid dynamics of the deconfined phase of the M5 brane theory on a Scherk-Schwarz circle.

Finally, we should point out that there has been a long history within the General Relativity literature of treating black hole horizons as surfaces associated with fluids. In one of the most recent discussion within this framework, the authors of [5] have modelled spinning black holes in $d+1$ dimensional (flat space) gravity by $d+1$ dimensional lumps of incompressible fluid; here the fluid surface represents the black hole horizon. Within this framework the 4+1 dimensional black ring, for instance, is modelled by a 4+1 dimensional stationary fluid lump of topology $B^3 \times S^1$ [6]. This description is rather different from the AdS/CFT induced description of black rings in Scherk Schwarz compactified AdS₅ as a 2+1 dimensional annulus of fluid. It would be interesting to better understand the interconnections between these approaches.

2 Fluid mechanics and thermodynamics

In this paper we study aspects of the dynamics of the deconfined plasma described in the previous section. A full accounting for the dynamics of the ‘gluon plasma’ is a very complicated problem. However, when the thermodynamic potentials and velocities vary over length scales large compared to the quasiparticle (‘gluon’) mean free path admit an effective description in terms of the equations of fluid dynamics. The variables in this description are the local values of the plasma or fluid velocity $u^\mu(x)$ and the plasma density $\rho(x)$ (the equation of state, as discussed in §§2.4, may be used to trade the density for the pressure or the temperature). The equations of fluid dynamics are simply a statement of the conservation of the stress tensor

$$\nabla_\mu T^{\mu\nu} = \partial_\mu T^{\mu\nu} + \Gamma_{\mu\lambda}^\mu T^{\lambda\nu} + \Gamma_{\mu\lambda}^\nu T^{\mu\lambda} = 0. \quad (5)$$

All input of the dynamical nature of the fluid that undergoes this flow appears in the specification of the stress tensor in terms of the velocity and density of the fluid, and from the thermodynamic equation of state (which determines the pressure and temperature as a function of density). In the rest of this brief subsection we describe the functional form of the fluid dynamical stress tensor for our plasma fluid in detail.

The stress tensor can be split into three parts:

$$T^{\mu\nu} = T_{\text{perfect}}^{\mu\nu} + T_{\text{dissipative}}^{\mu\nu} + T_{\text{surface}}^{\mu\nu}.$$

The first part, $T_{\text{perfect}}^{\mu\nu}$, is the stress tensor for a perfect fluid with no dissipative forces. It is a function only of fluid velocity and thermodynamic quantities in the rest frame, and not of their space time derivatives.

The second part, $T_{\text{dissipative}}^{\mu\nu}$, receives contributions from viscosity and heat flow. In the long wavelength limit this piece is linear in the first derivatives of the velocity and temperature.

The third part, $T_{\text{surface}}^{\mu\nu}$, represents surface contributions to the stress tensor, and requires more explanation. Any fluid configuration with a surface has large variations in (for instance) the fluid density over the scale of the mean free path, in directions normal to the surface (see for instance [2]). As a consequence it is impermissible to use the Navier-Stokes equations for the fluid in the neighbourhood of the surface. When the deviations of the surface from a straight line are small over length scale of the mean free path, however, all effects of the surface may approximately be captured by a delta function localised ‘surface tension’ contribution, $T_{\text{surface}}^{\mu\nu}$, to the stress tensor. In the long wavelength approximation, this term depends only on the gradients of the surface and not its curvature.

2.1 Perfect fluid stress tensor

The most general ultralocal stress tensor one can build out of the fluid velocity and thermodynamic quantities that reduces to what is expected for a fluid at rest is [7, ch.22]

$$T_{\text{perfect}}^{\mu\nu} = (\rho + P)u^\mu u^\nu + P g^{\mu\nu}. \quad (6)$$

2.2 Dissipative part

Realistic fluids have a dissipative component to their stress tensor in addition to the perfect fluid piece. In the long wavelength limit, this stress tensor is a function of the acceleration, expansion, projection, and shear tensors (see e.g. [7, Exercise 22.6-7] and references therein),

$$\begin{aligned} a^\mu &= u^\nu \nabla_\nu u^\mu, \\ \theta &= \nabla_\mu u^\mu, \\ P^{\mu\nu} &= g^{\mu\nu} + u^\nu u^\mu, \\ \sigma^{\mu\nu} &= \frac{1}{2} (P^{\mu\lambda} \nabla_\lambda u^\nu + P^{\nu\lambda} \nabla_\lambda u^\mu) - \frac{1}{d-1} \theta P^{\mu\nu}. \end{aligned} \quad (7)$$

In terms of these quantities and the heat flow vector q^μ (see immediately below)

$$T_{\text{dissipative}}^{\mu\nu} = -\zeta \theta P^{\mu\nu} - 2\eta \sigma^{\mu\nu} + q^\mu u^\nu + u^\mu q^\nu, \quad (8)$$

where ζ is the bulk viscosity, η is the shear viscosity. The heat flux vector,

$$q^\mu = -\kappa P^{\mu\nu} (\partial_\nu \mathcal{T} + a_\nu \mathcal{T}). \quad (9)$$

is the relativistic generalisation of $\vec{q} = -\kappa \vec{\nabla} \mathcal{T}$ (here κ is the thermal conductivity); the extra term in (9) is related to the inertia of flowing heat.

2.3 Surface contribution

We will use a simple model of surface tension where the energy stored in the surface and the force per unit length are both given by σ , which we take to be the surface tension

at the critical temperature computed in [2]. We will ignore any dependence σ could have on the fluid temperature. This approximation is valid when the fluid temperature at the surface does not deviate substantially from \mathcal{T}_c .

Consider a localised lump of fluid whose surface in space is given by the equation $f(x) = 0$. The surface contribution to the stress tensor will be proportional to $\sigma\delta(f)$. In the long wavelength limit it will only depend on the first derivatives of f . The most general stress tensor we can build is

$$T_{\text{surface}}^{\mu\nu} = [\alpha \partial^\mu f \partial^\nu f + \beta u^\mu u^\nu + \gamma (u^\mu \partial^\nu f + \partial^\mu f u^\nu) + \delta g^{\mu\nu}] \sigma \delta(f).$$

As $u^2 = -1$ and $u^\mu \partial_\mu f = 0$ (the surface moves with the fluid), the only invariant quantity that $\alpha, \beta, \gamma, \delta$ can depend on is $(\partial^\mu f \partial_\mu f)$. We can fix this dependence by demanding invariance under reparameterisations of the surface⁵ (e.g. $f(x) \rightarrow g(x)f(x)$, so that $\partial f \rightarrow g\partial f + f\partial g = g\partial f$ at the surface). Defining $f_\mu = \frac{\partial_\mu f}{\sqrt{\partial f \partial f}}$:

$$T_{\text{surface}}^{\mu\nu} = [A f^\mu f^\nu + B u^\mu u^\nu + C (u^\mu f^\nu + f^\mu u^\nu) + D g^{\mu\nu}] \sigma \sqrt{\partial f \cdot \partial f} \delta(f).$$

We can fix A, B, C, D by looking at a fluid at rest, $u^\mu = (1, 0, 0, \dots)$, with a surface $f(x) = x$

$$T_{\text{surface}}^{\mu\nu} = \begin{pmatrix} B - D & C & 0 \\ C & A + D & 0 \\ 0 & 0 & D \end{pmatrix} \sigma \delta(x) = \begin{pmatrix} 1 & 0 & 0 \\ 0 & 0 & 0 \\ 0 & 0 & -1 \end{pmatrix} \sigma \delta(x).$$

This gives

$$T_{\text{surface}}^{\mu\nu} = \sigma [f^\mu f^\nu - g^{\mu\nu}] \sqrt{\partial f \cdot \partial f} \delta(f). \quad (10)$$

2.4 Equations of state

To solve the equations of fluid mechanics, one also needs expressions for the various coefficients that appear in the stress tensor above in terms of the density. For our purposes, we only need to know the thermodynamic properties of the fluid, which could be determined from the static black brane solution (3). In this subsection we discuss the free energy, temperature etc. of the plasma at rest. This is different from the free energy, temperature etc. of the plasmaball/plasmaring.

For a conformal theory in d dimensions with no conserved charges, dimensional analysis and extensivity determine

$$\mathcal{F} = -\alpha V \mathcal{T}^d, \quad (11)$$

with α an arbitrary constant. In our situation, the plasma is dual to the same black brane, so it doesn't know about any capping off in the IR except that the energy is measured with respect to a different zero. Before reducing on the Scherk-Schwarz circle, it behaves like

⁵However, we should choose a parametrisation such that $\partial_\mu f$ is well behaved at the surface, e.g. $f = x$, but not $f = x^2$ or $f = \sqrt{x}$.

a conformal theory in $d + 1$ dimensions plus a vacuum energy density. After dimensional reduction⁶, we have

$$\mathcal{F} = V (\rho_0 - \alpha \mathcal{T}^{d+1}). \quad (12)$$

This gives

$$\begin{aligned} P &= - \left(\frac{\partial \mathcal{F}}{\partial V} \right)_{\mathcal{T}} = \alpha \mathcal{T}^{d+1} - \rho_0, \\ \mathcal{S} &= - \left(\frac{\partial \mathcal{F}}{\partial \mathcal{T}} \right)_{V} = (d + 1) \alpha V \mathcal{T}^d, \\ \mathcal{E} &= \mathcal{F} + \mathcal{T} \mathcal{S} = V (\rho_0 + d \alpha \mathcal{T}^{d+1}). \end{aligned} \quad (13)$$

In terms of intensive quantities, we have

$$\begin{aligned} P &= \frac{\rho - (d + 1) \rho_0}{d}, & P + \rho &= \left(\frac{d + 1}{d} \right) (\rho - \rho_0), \\ s &= (d + 1) \alpha^{1/(d+1)} \left(\frac{\rho - \rho_0}{d} \right)^{d/(d+1)}, & \mathcal{T} &= \left(\frac{\rho - \rho_0}{d \alpha} \right)^{1/(d+1)}, \end{aligned} \quad (14)$$

or, in three dimensions

$$\begin{aligned} P &= \frac{\rho - 4\rho_0}{3}, & P + \rho &= \frac{4}{3} (\rho - \rho_0), \\ s &= \frac{4\alpha^{1/4}}{3^{3/4}} (\rho - \rho_0)^{3/4}, & \mathcal{T} &= \left(\frac{\rho - \rho_0}{3\alpha} \right)^{1/4}. \end{aligned} \quad (15)$$

Note that the critical density and temperature are those for which the pressure is zero

$$\rho_c = (d + 1) \rho_0, \quad \mathcal{T}_c = \left(\frac{\rho_0}{\alpha} \right)^{1/(d+1)}. \quad (16)$$

For the black-brane equation of state (4)

$$\rho_0 = \frac{\pi^2 N^2 \mathcal{T}_c^3}{8}, \quad \alpha = \frac{\pi^2 N^2}{8 \mathcal{T}_c}. \quad (17)$$

However, the values of these constants will not be important below.

3 Rigidly rotating configurations

In this section, we study stationary, axially symmetric rotating fluid configurations, whose equation of state is presented in various forms in §§2.4. We choose the axis of rotation as our

⁶Strictly speaking, it is not a dimensional reduction as we will have plasma temperature of the same order as the Kaluza-Klein scale. Rather, we are restricting attention to classical solutions that do not vary in this compact dimension.

origin in polar coordinates; in these coordinates the fluid density is a function only of the radial coordinate r , and the (t, r, ϕ) components of the velocity are given by $u^\mu = \gamma(1, 0, \omega)$ with $\gamma = (1 - \omega^2 r^2)^{-1/2}$. We will find two distinct kinds of solutions; rotating plasmaballs with the topology of a two dimensional disk, and plasmarings with the topology of a two dimensional annulus. The configurations we find are exact solutions to the equations of relativistic fluid dynamics; in §§5.2 we will demonstrate that these equations accurately represent plasma dynamics for large enough plasmaballs and plasmarings.

3.1 Equations of motion

Our fluid propagates in flat 2+1 dimensional space. In polar coordinates

$$ds^2 = -dt^2 + dr^2 + r^2 d\phi^2. \quad (18)$$

This gives the following non-zero Christoffel symbols:

$$\Gamma_{\phi\phi}^r = -r \quad \Gamma_{r\phi}^\phi = \Gamma_{\phi r}^\phi = \frac{1}{r}. \quad (19)$$

For the stationary, axially symmetric configurations under consideration, $\partial_t T^{\mu\nu} = \partial_\phi T^{\mu\nu} = 0$. Using (19), (5) becomes

$$0 = \nabla_\mu T^{\mu t} = \partial_r T^{rt} + \frac{1}{r} T^{rt}, \quad (20)$$

$$0 = \nabla_\mu T^{\mu r} = \partial_r T^{rr} + \frac{1}{r} T^{rr} - r T^{\phi\phi}, \quad (21)$$

$$0 = \nabla_\mu T^{\mu\phi} = \partial_r T^{r\phi} + \frac{3}{r} T^{r\phi}. \quad (22)$$

The boundaries are $f_n = r - r_n$, with n labelling the different boundaries (outer for the disk, outer and inner for the annulus). The ‘perfect fluid part’ of the stress tensor is

$$T_{\text{perfect}}^{\mu\nu} = \begin{pmatrix} \gamma^2(\rho + \omega^2 r^2 P) & 0 & \gamma^2 \omega(\rho + P) \\ 0 & P & 0 \\ \gamma^2 \omega(\rho + P) & 0 & \frac{\gamma^2}{r^2}(\omega^2 r^2 \rho + P) \end{pmatrix} \quad (23)$$

and the surface stress tensor

$$T_{\text{surface}}^{\mu\nu} = \sigma \sum_n \delta(r - r_n) \begin{pmatrix} 1 & 0 & 0 \\ 0 & 0 & 0 \\ 0 & 0 & -\frac{1}{r^2} \end{pmatrix} \quad (24)$$

For the dissipative part of the stress tensor, we find $\theta = \sigma^{\mu\nu} = 0$ and

$$\partial_\nu \mathcal{T} + a_\nu \mathcal{T} = \left(0, \gamma \frac{d}{dr} \left[\frac{\mathcal{T}}{\gamma} \right], 0 \right), \quad (25)$$

so that

$$T_{\text{dissipative}}^{\mu\nu} = -\kappa\gamma^2 \frac{d}{dr} \left[\frac{\mathcal{T}}{\gamma} \right] \begin{pmatrix} 0 & 1 & 0 \\ 1 & 0 & \omega \\ 0 & \omega & 0 \end{pmatrix} \quad (26)$$

We will now write the equations of motion $\nabla_\mu T^{\mu\nu} = 0$ temporarily ignoring the contribution from this heat flow, $T_{\text{dissipative}}^{\mu\nu}$; it will turn out (we see this immediately below) that $T_{\text{dissipative}}^{\mu\nu}$ actually vanishes on our solutions, justifying this procedure.

The only non-trivial equation of motion, (21), can be written as

$$\frac{dP}{dr} = \frac{\omega^2 r}{1 - \omega^2 r^2} (\rho + P) - \sum_n \frac{\sigma}{r} \delta(r - r_n). \quad (27)$$

For these fluids (with no chemical potentials for any conserved charges), $P = -f$ is a function only of \mathcal{T} , so $P + \rho = s\mathcal{T}$ and $\frac{dP}{d\mathcal{T}} = s$. So, away from the boundaries, (27) becomes

$$\begin{aligned} s \frac{d\mathcal{T}}{dr} &= s\mathcal{T} \frac{d \ln \gamma}{dr} \\ \implies \frac{d}{dr} \left[\frac{\mathcal{T}}{\gamma} \right] &= 0 \end{aligned} \quad (28)$$

It follows that $T_{\text{dissipative}}^{\mu\nu}$ vanishes for rigid rotation, justifying our neglect of heat flow.

Our discussion has not assumed a specific form of the equation of state. Using this particular equation of state of our plasma (15), we can rewrite (28) in the fluid interior as

$$(\rho(r) - \rho_0) (1 - \omega^2 r^2)^2 = \text{constant}. \quad (29)$$

Integrating (27) across a surface gives

$$P_{>} - P_{<} = -\frac{\sigma}{r}. \quad (30)$$

where $P_{>}$ and $P_{<}$ are the pressures at infinitesimally greater and smaller radii than the location of the surface.

3.2 Spinning ball

Let us first study a fluid configuration with a single outer surface at $r = r_o$ with $P_{>} = 0$. Using the equation of state (15), the boundary condition (30) can be written as

$$\rho(r_o) = 4\rho_0 + \frac{3\sigma}{r_o}. \quad (31)$$

If we define dimensionless variables

$$\tilde{\omega} = \frac{\sigma\omega}{\rho_0}, \quad \tilde{r} = \frac{\rho_0 r}{\sigma}, \quad v = \omega r = \tilde{\omega} \tilde{r}, \quad (32)$$

then (29) can be written as

$$\left(\frac{\rho(v) - \rho_0}{3\rho_0}\right) (1 - v^2)^2 = \left(1 + \frac{\tilde{\omega}}{v_o}\right) (1 - v_o^2)^2 \equiv g_+(v_o). \quad (33)$$

Note that the range of v is $[0, 1]$ and $\rho(v) - \rho_0$ is always positive for this solution, as is required for the last equation of (15) to make sense.

We can also compute the local plasma temperature using (15)

$$\mathcal{T} = \gamma \left(\frac{\rho_0 g_+(v_o)}{\alpha}\right)^{1/4}. \quad (34)$$

3.3 Spinning ring

We now turn to solutions that have an inner surface well an outer surface. In addition to the boundary condition at the outer radius (31) we now have

$$\rho(r_i) = 4\rho_0 - \frac{3\sigma}{r_i}. \quad (35)$$

So the full solution is

$$\begin{aligned} \left(\frac{\rho(v) - \rho_0}{3\rho_0}\right) (1 - v^2)^2 &= \left(1 + \frac{\tilde{\omega}}{v_o}\right) (1 - v_o^2)^2 \equiv g_+(v_o) \\ &= \left(1 - \frac{\tilde{\omega}}{v_i}\right) (1 - v_i^2)^2 \equiv g_-(v_i). \end{aligned} \quad (36)$$

Note that $\rho(v) - \rho_0 \geq 0$ provided that $v_i \geq \tilde{\omega}$.

Again, we can compute the local plasma temperature using (15)

$$\mathcal{T} = \gamma \left(\frac{\rho_0 g_+(v_o)}{\alpha}\right)^{1/4} = \gamma \left(\frac{\rho_0 g_-(v_i)}{\alpha}\right)^{1/4}. \quad (37)$$

The two functions, $g_{\pm}(v)$ are schematically plotted in fig.3 for some value of $\tilde{\omega}$, where we have labelled special velocities v_i^* and v_o^* . As $v_i < 1$, it is necessary that $\tilde{\omega} < 1$.

We can see that there are no solutions to $g_+(v_o) = g_-(v_i)$ for $v_o < v_o^*$ and two solutions for $v_o > v_o^*$. One of these has $v_i < v_i^*$ (the thick ring) and one has $v_i > v_i^*$ (the thin ring). The distinction between ‘thin’ and ‘thick’ rings will not prove physically important. In §5.1 we will find it physically useful to distinguish between distinct ring solutions (we will call these large and small rings) at the same values of conserved charges (energy and angular momentum), rather than the parameters v_o and $\tilde{\omega}$.

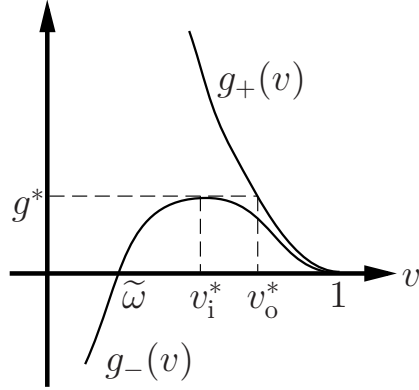


Figure 3: Graph of $g_{\pm}(v)$ showing possible values of $v_{o,i}$

4 Thermodynamic Potentials

In this section, we compute the thermodynamic potentials (energy, angular momentum, entropy, etc.) for the spinning plasmaball and plasmaring themselves, rather than their constituent plasma. This includes contributions from the kinetic energy of the plasma as well as its internal energy.

The constitutive relations we find are predictions for, e.g., entropy as a function of mass and angular momentum of the dual gravity solutions.

4.1 Densities

In this subsection we list formulae for energy density, angular momentum density and entropy density. In the next subsection we will integrate these expressions to find explicit formulae for the energy, angular momentum and entropy of spinning plasmaballs and plasmarings.

The energy density is given by

$$\begin{aligned} T^{tt} &= \gamma^2 (\rho + \omega^2 r^2 P) + \sum_n \sigma \delta(r - r_n) \\ &= \rho_0 \left[1 + g_+(v_o) \frac{3 + v^2}{(1 - v^2)^3} + \sum_n 2\tilde{\omega} v \delta(v^2 - v_n^2) \right]. \end{aligned} \quad (38)$$

The angular momentum density is given by

$$r^2 T^{t\phi} = \gamma^2 \omega r^2 (\rho + P) = 4\sigma \frac{g_+(v_o)}{\tilde{\omega}} \frac{v^2}{(1 - v^2)^3}. \quad (39)$$

The entropy density is given by

$$\gamma_s = \frac{4\alpha^{1/4} (\rho - \rho_0)^{3/4}}{3^{3/4} \sqrt{1 - v^2}} = 4(\alpha\rho_0^3)^{1/4} \frac{g_+(v_o)^{3/4}}{(1 - v^2)^2} \quad (40)$$

4.2 Integrals

We can define some dimensionless variables

$$\tilde{E} = \frac{\rho_0 E}{\pi \sigma^2}, \quad \tilde{L} = \frac{\rho_0^2 L}{\pi \sigma^3}, \quad \tilde{S} = \frac{\rho_0^{5/4} S}{\pi \alpha^{1/4} \sigma^2}, \quad \tilde{T} = T \left(\frac{\alpha}{\rho_0} \right)^{1/4}, \quad \tilde{\Omega} = \frac{\sigma \Omega}{\rho_0}. \quad (41)$$

The last of these ensure that $\tilde{T} = \left(\frac{\partial \tilde{E}}{\partial \tilde{S}} \right)_{\tilde{L}}$ and $\tilde{\Omega} = \left(\frac{\partial \tilde{E}}{\partial \tilde{L}} \right)_{\tilde{S}}$ follow from $T = \left(\frac{\partial E}{\partial S} \right)_L$ and $\Omega = \left(\frac{\partial E}{\partial L} \right)_S$

4.2.1 Spinning ball

Energy

$$\tilde{E} = \frac{4v_o^2 - v_o^4 + 5\tilde{\omega}v_o - \tilde{\omega}v_o^3}{\tilde{\omega}^2} \quad (42)$$

Angular momentum

$$\tilde{L} = \frac{2v_o^4 + 2\tilde{\omega}v_o^3}{\tilde{\omega}^3} \quad (43)$$

Entropy

$$\tilde{S} = \frac{4v_o^2}{\tilde{\omega}^2} \sqrt{1 - v_o^2} \left(1 + \frac{\tilde{\omega}}{v_o} \right)^{3/4} \quad (44)$$

4.2.2 Spinning ring

Energy

$$\tilde{E} = \frac{4(v_o^2 - v_i^2) - (v_o^4 - v_i^4) + 5\tilde{\omega}(v_o + v_i) - \tilde{\omega}(v_o^3 + v_i^3)}{\tilde{\omega}^2} \quad (45)$$

Angular momentum

$$\tilde{L} = \frac{2(v_o^4 - v_i^4) + 2\tilde{\omega}(v_o^3 + v_i^3)}{\tilde{\omega}^3} \quad (46)$$

Entropy

$$\tilde{S} = \frac{4}{\tilde{\omega}^2} \left[\sqrt{1 - v_o^2} \left(1 + \frac{\tilde{\omega}}{v_o} \right)^{3/4} - \sqrt{1 - v_i^2} \left(1 - \frac{\tilde{\omega}}{v_i} \right)^{3/4} \right] \quad (47)$$

4.3 Temperature and angular velocity

In this subsection we determine the temperature and angular velocity of spinning plasma-balls and plasmarings using

$$\tilde{T} = \left(\frac{\partial \tilde{E}}{\partial \tilde{S}} \right)_{\tilde{L}}, \quad \tilde{\Omega} = \left(\frac{\partial \tilde{E}}{\partial \tilde{L}} \right)_{\tilde{S}}. \quad (48)$$



Figure 4: Scatter plots of energy and angular momentum of (a) spinning balls and (b) rings.

Note that the temperature defined above is different from the local plasma temperature, \mathcal{T} (which varies across our solutions), in (13-15); the angular velocity defined above will turn out to be ω on all our solutions, although it is apparently a priori different.

It may be verified that the temperature and angular velocity of plasmaballs is given by

$$\tilde{T} = [g_+(v_o)]^{1/4}, \quad \tilde{\Omega} = \tilde{\omega}. \quad (49)$$

The corresponding expressions for the rings are identical

$$\tilde{T} = [g_+(v_o)]^{1/4} = [g_-(v_i)]^{1/4}, \quad \tilde{\Omega} = \tilde{\omega}. \quad (50)$$

Thus, local temperatures, \mathcal{T}_c , and angular velocities, ω , for both the ball and the ring, are given simply in terms of T and Ω

$$\mathcal{T} = \frac{T}{\sqrt{1-v^2}}, \quad \omega = \Omega.$$

5 Solutions at fixed energy and angular momentum

5.1 Existence

In fig.4, we display scatter plots for the energy and angular momentum of ball and ring solutions over the full range of solution parameters.⁷ The various regions of existence of the plasmaball, thin plasmaring and thick plasmaring in the $E - L$ plane are drawn schematically in fig.5.

The ball solution exists over a region C in the $E - L$ plane. At the boundary of the region C the ball solution v_o attains its maximum value of unity. Using (42,43) we find an analytic expression for the boundary of C:

$$\tilde{L} = \frac{2}{27} \left[(3\tilde{E} + 4)^{3/2} - 9\tilde{E} - 8 \right] \sim \frac{2\tilde{E}^{3/2}}{3^{3/2}} \quad \text{for large } \tilde{E}. \quad (51)$$

⁷In order to generate these plots for the ball, a range of values of $(v_o, \tilde{\omega})$ were chosen and (E, L) were computed using (42,43). For the ring, a range of values of $(v_i, \tilde{\omega})$ were chosen, v_o was computed using (36), and (E, L) were computed using (45,46).

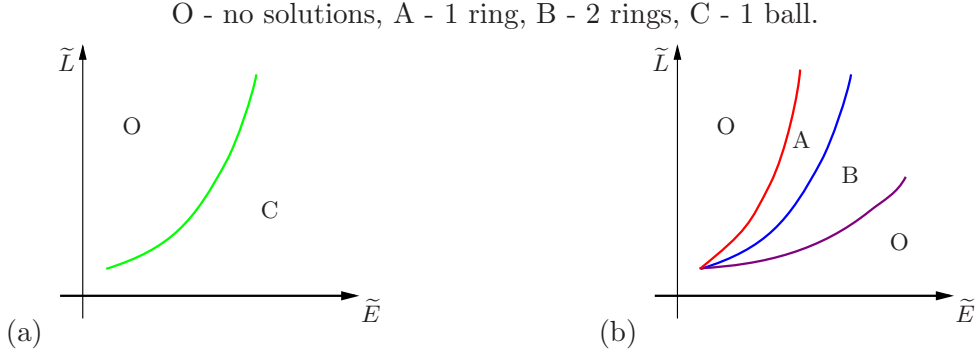


Figure 5: Regions where (a) ball and (b) ring solutions exist.

From (49), we see that balls on this boundary saturate the extremality bound (i.e. have zero temperature).

Like the balls, rings of a fixed energy have a maximum value of angular momentum. Rings at the edge of this bound (the boundary between O and A in fig.5b) have $v_o = v_i = 1$ and so are extremal (see (50)) and of zero width. Using (45,46) the O-A boundary is given by

$$\tilde{L} = \frac{\tilde{E}^2}{16}, \quad (52)$$

(this expression is valid only for $\tilde{E} > 8$, $\tilde{L} > 2$; at lower energies $\tilde{\omega}$ exceeds unity).

As we lower angular momentum of the solution, this ring moves away from extremality and increases in width. At a particular angular momentum (the boundary between region A and region B) a new ring solution comes into existence. The corresponding solution has $v_o = 1$, $v_i = \tilde{\omega}$ and so is extremal (see (50)). Using (45,46), the analytic expression for the A-B boundary is given by

$$\tilde{L} = \frac{2}{27} \left[(3\tilde{E} + 1)^{3/2} - 9\tilde{E} + 1 \right] \sim \frac{2\tilde{E}^{3/2}}{3^{3/2}} \quad \text{for large } \tilde{E}, \quad (53)$$

(for $\tilde{E} > 8$, $\tilde{L} > 2$ as above). In the high energy limit $\tilde{E} \gg 1$ the ratio of angular momentum for the new extremal rings (at the A-B boundary) and extremal plasmaball tends to unity, (even though the the difference between angular momenta does not go to zero). Consequently the leading high energy behaviour of (53) and (51) is the same in this limit, as is also clear from fig.7. We emphasise that, for our solutions, the extremal ball and extremal thick ring are not quite identical (as is the case for black holes and small black rings [8] in flat space) as the inner radius of our extremal thick rings does not vanish. However, the inner radius of the extremal thick ring is always (for all values of energy) of the same order as the thickness of the domain wall. As the fluid dynamics approximations fail precisely under these conditions, it could well be that the new extremal plasmaring and extremal plasmaball are actually identical configurations.

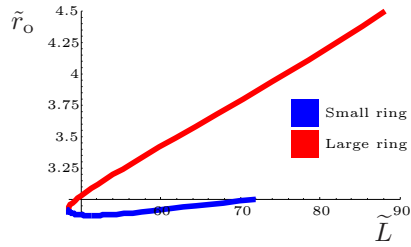


Figure 6: Outer radius of large and small rings as a function of angular momentum, \tilde{L} , at fixed energy, $\tilde{E} = 40$.

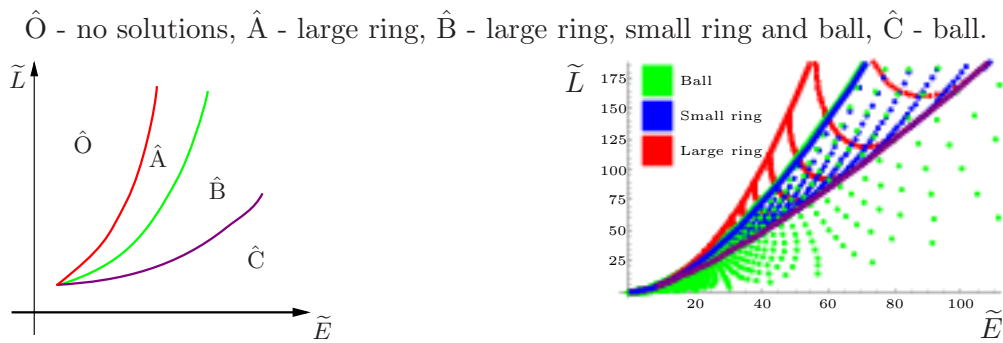


Figure 7: Regions where ball and ring solutions exist.

As we further lower angular momentum, the new ring solution moves away from extremality; this new solution always has a smaller outer radius than the ‘original’ ring solution (the solutions that also exists in region A), as shown in fig.6. As a consequence, we refer to these two ring solutions as small and large respectively.

Further lowering angular momentum, we hit the boundary between regions B and O where the two ring solutions merge into each other. At still lower angular momentum, we have no ring solutions. The C-O boundary may thus be obtained by minimising \tilde{L} at fixed \tilde{E} . If one uses (36) to eliminate $\tilde{\omega}$, this amounts to

$$\left(\frac{\partial \tilde{E}}{\partial v_o} \right)_{v_i} \left(\frac{\partial \tilde{L}}{\partial v_i} \right)_{v_o} - \left(\frac{\partial \tilde{E}}{\partial v_i} \right)_{v_o} \left(\frac{\partial \tilde{L}}{\partial v_o} \right)_{v_i} = 0.$$

The existence of plasmaball and plasmaring solutions in the E-L plane may thus be summarised as in fig.7.

5.2 Validity

As we have described above, plasmaballs and plasmarings are exact solutions to the relativistic Navier-Stokes equations (supplemented by sharp surface boundary conditions).

However these equations of fluid dynamics accurately capture the dynamics of the fluid plasma only under certain conditions. In our discussion we have assigned a well defined pressure and temperature to the fluid at each point in space. Clearly this procedure is valid only when the variation of these thermodynamic quantities is small over the length scale of the mean free path of the quasiparticles (roughly gluons) of our system. The mean free path is of the same order as the mass gap of the theory, which in turn is similar to the deconfinement temperature.⁸

Second, we have treated the surface of the plasma as sharp; in reality this surface has a thickness of order \mathcal{T}_c^{-1} . Consequently, our treatment of the surface is valid only when its deviation from a straight line occurs on scales large compared to \mathcal{T}_c^{-1} (higher derivative contributions to the surface stress tensor, which we have ignored in our treatment, would become important if this were not the case); further we must also require that only a small fraction of the fluid should reside in surfaces.

Thirdly, we have ignored the fact that the surface tension is a function of the fluid temperature at the surface, and simply set $\sigma = \sigma(\mathcal{T}_c)$. This is valid provided that $\mathcal{T}/\mathcal{T}_c \approx 1$ at all surfaces.

Finally, the fluid evolution equations, by their very nature, track mean velocities and energy densities, ignoring fluctuations. In our context this approximation is justified by large N ; fluctuations are suppressed by powers of $1/N^2$, dual to the suppression of quantum metric fluctuations in the bulk.

Recall that

$$\rho_0 \sim N^2 \mathcal{T}_c^3, \quad \sigma \sim N^2 \mathcal{T}_c^2, \quad \text{so} \quad \frac{1}{\mathcal{T}_c} \sim \frac{\sigma}{\rho_0}$$

(for the domain wall solution of [2], $\frac{\sigma}{\rho_0} = 2.0 \times \frac{4}{\mathcal{T}_c}$ and the thickness is $6 \times \frac{1}{2\pi\mathcal{T}_c}$).

As an estimate of the scale over which thermodynamic quantities vary, we compute the fractional change in the fluid temperature over the distance of a mean free path. As the temperature is proportional to γ , we should look at

$$\frac{1}{\mathcal{T}_c} \frac{d}{dr} \ln \gamma \sim \frac{\sigma}{\rho_0} \frac{\omega^2 r}{1 - \omega^2 r^2} = \frac{\tilde{\omega} v}{1 - v^2}.$$

As this takes its maximum value at the outer surface, the condition for the validity of the equations of fluid dynamics may be estimated to be

$$\Delta u \equiv \frac{\tilde{\omega} v_o}{1 - v_o^2} \ll 1. \tag{54}$$

Our treatment of the surface as a zero-thickness object is valid if

$$\{r_o, r_i, r_o - r_i\} \gg \frac{1}{\mathcal{T}_c} \sim \frac{\sigma}{\rho_0}$$

⁸It was argued in [2] that the mean free path does not scale with N . According to quasiparticle kinetic theory, the mean free path is approximately the ratio of the shear viscosity and the energy density. The computations reviewed in [3] show that this quantity is of order $1/\mathcal{T}_c$ in the limit of the 't Hooft coupling $\lambda \rightarrow \infty$.

(for the ring, the r_o inequality in the equation above follows automatically from the either of the other two inequalities). This condition can be rewritten in terms of our dimensionless variables as

$$\begin{aligned} v_o \gg \tilde{\omega} & \quad \text{or} & \quad \tilde{r}_o \gg 1 & \quad \text{for the ball,} \\ \{v_i, v_o - v_i\} \gg \tilde{\omega} & \quad \text{or} & \quad \{\tilde{r}_i, \tilde{r}_o - \tilde{r}_i\} \gg 1 & \quad \text{for the ring.} \end{aligned} \tag{55}$$

In fig.8, we have plotted $\ln(1/\Delta u)$, $\ln(\tilde{r}_i)$, $\ln(\tilde{r}_o - \tilde{r}_i)$ and $\ln(\tilde{r}_o)$ for the thin ring, thick ring and ball. From the figure we observe that these quantities are large (and so the fluid dynamics approximations of this paper are accurate) when our rings and balls have large energy and we stay away from the extremality bounds.

Finally, validity of our approximation of the surface tension as a constant (independent of temperature) requires that the maximum and minimum values of $\ln(\mathcal{T}/\mathcal{T}_c)$ (which occur at the outer and inner surfaces respectively) are both small. We have plotted these quantities in fig.9. It is clear from these figures that this condition is fulfilled for large energy and angular momentum provided that we are not near extremality.

5.3 Global stability and phase diagram

Recall that (see fig.7) at fixed values of energy and angular momentum, we have either 0, 1 or 3 plasmaball / plasmaring solutions. At those values of charges for which multiple solutions exist, it is natural to inquire which of these solutions is entropically favoured. In fig.10(a) we have plotted the entropy of plasma ball and plasmaring solutions as a function of angular momentum at fixed energy.

Note that, when it exists, the small ring always carries lower entropy than both the big ring and the plasmaball. At low enough angular momentum the plasmaball is the only solution. This solution continues to be entropically dominant (upon raising the angular momentum) over an interval, even after the new ring solutions are nucleated. At a critical angular momentum, however, the entropy of the large ring equals and then exceeds the entropy of the plasmaball (all three ring solutions continue to exist in a neighbourhood about this point). The large ring is the entropically dominant solution at all larger angular momenta.

The phase boundary can be seen in fig.10(b).

5.4 Comparison with black rings in flat 5D space

As we have explained in the introduction, the plasmaball and plasmaring solutions of this paper are dual to black holes and black rings in the background (1). Unfortunately the corresponding gravitational solutions have not yet been constructed; however exact Black ring solutions to the vacuum Einstein equations in 5 dimensions, were obtained in [8] (see [9] for a review). These solutions were further studied in [10]. In this subsection we compare the properties these black rings and black holes with our plasmaballs and plasmarings, and

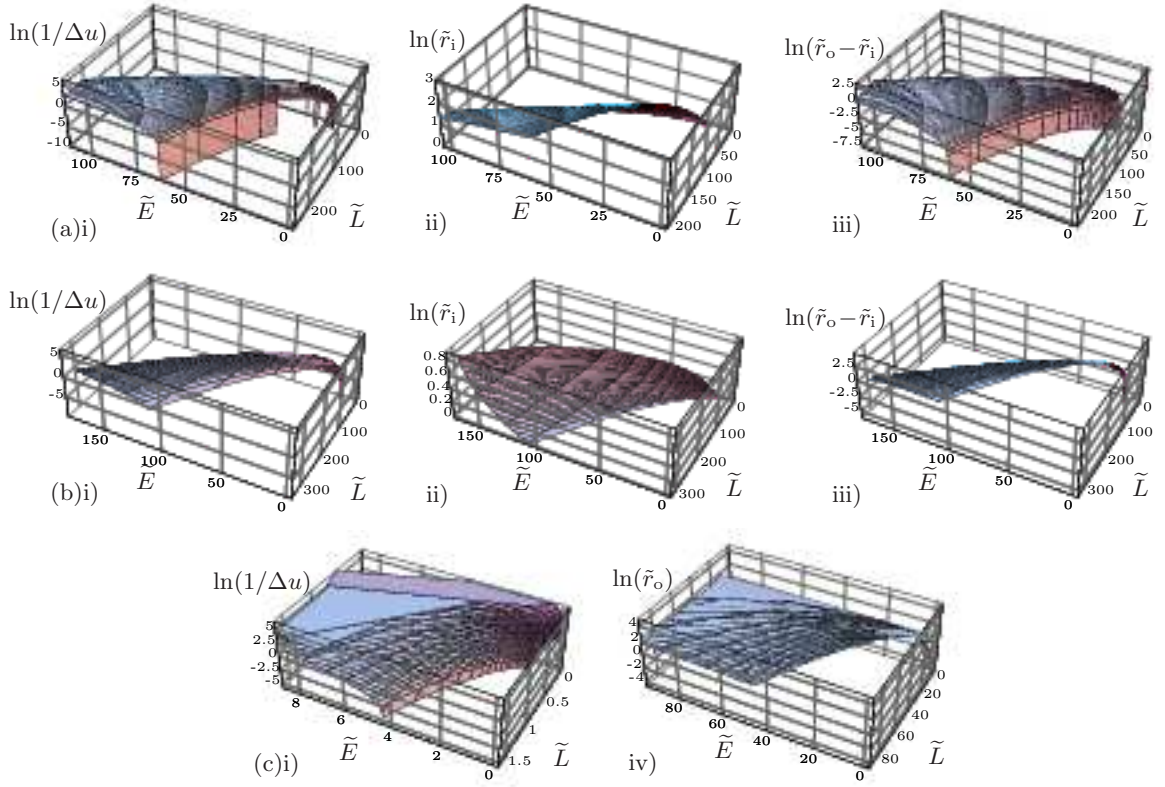


Figure 8: Plots of i) $\ln(1/\Delta u)$ ii) $\ln(\tilde{r}_i)$, iii) $\ln(\tilde{r}_o - \tilde{r}_i)$, iv) $\ln(\tilde{r}_o)$ for (a) large rings, (b) small rings and (c) balls.

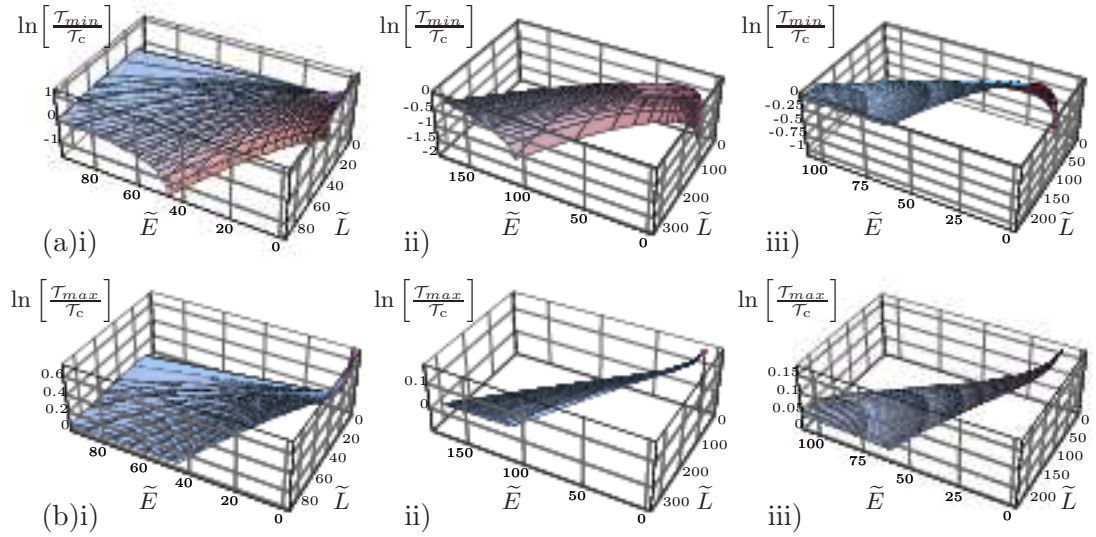


Figure 9: Plots of (a) $\ln(\mathcal{T}_{min}/\mathcal{T}_c)$ (b) $\ln(\mathcal{T}_{max}/\mathcal{T}_c)$ for i) balls, ii) small rings, iii) large rings.

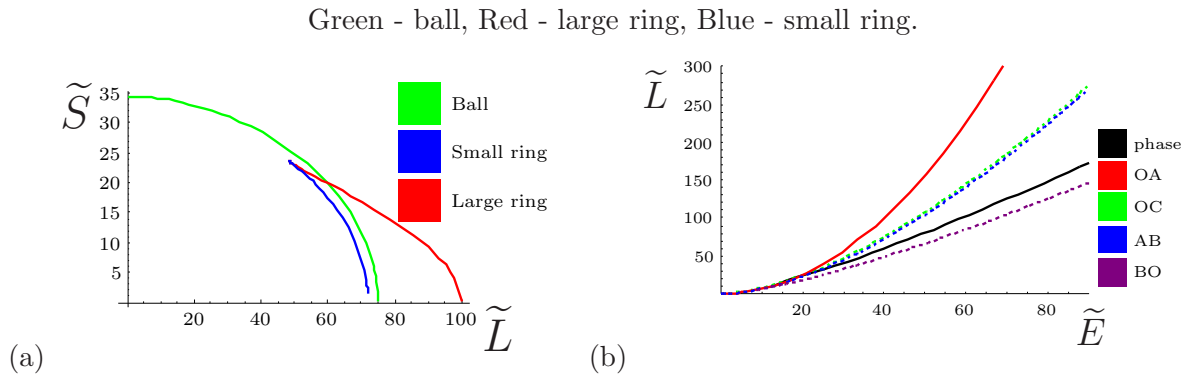


Figure 10: (a) Entropy, \tilde{S} , as a function of angular momentum, \tilde{L} for fixed energy, $\tilde{E} = 40$. (b) Phase boundary with existence boundaries.

find broad qualitative agreement between the two.⁹

In fig.11 we have presented a schematic plot for the existence of black hole and black ring solutions in 5 dimensional flat space. This figure looks fairly similar to figs.7,10(b). The major qualitative difference is the absence of the analogue of the region O (see fig. 7) in fig. 11. Thus unlike thin black rings in flat 5 dimensional space, plasmarrings (and so black rings in Scherk-Schwarz AdS_5) have an upper bound to their angular momentum at fixed energy.¹⁰

It is interesting to pursue the comparison between these solutions in more detail. The gravitational analogue of fig.10 (presented as [8, fig.3]) looks fairly similar to our figure. The main qualitative differences are: unlike for plasmarrings, the entropy of the large flat space black ring doesn't go to zero at a finite angular momentum (it asymptotes to zero at infinity) and the entropy of the small flat space black ring and black hole go to zero at exactly the same point instead of the slightly different values that we see. We expect that first of these differences reflects a physical difference between black rings in flat space and Scherk-Schwarz compactified AdS_5 , the second difference is an artefact of the breakdown of the fluid dynamics approximation for extremal small rings (whose inner radius is always of order the mean free path).

In even greater detail, we could quantitatively compare the boundaries between regions O, A, B and C (see fig.5). These curves, as well as the phase boundary, may be parameterised by $L = xE^y$ at large energies.

For black holes and black rings in flat space $y_{AB} = y_{OC} = y_{BO} = y_{phase} = \frac{3}{2}$. For our plasmaballs and plasmarrings, as one can see in fig.12 (or from (51-53) for the first three), for large energy, we get $y_{OA} = 2$, $y_{AB} = y_{OC} = \frac{3}{2}$, $y_{BO} = 1.25$ and $y_{phase} = 1.25$ (see table

⁹While we expect the properties of plasmaballs and plasmarrings to match quantitatively with those of black holes and black rings in the background (1), we could not hope to find better than qualitative agreement with the properties of the same objects in flat space.

¹⁰This upper bound was expected for black rings in AdS. The negative cosmological constant has a similar effect to the dipole charge of [11]. We thank R. Emparan for explaining this to us.

A' - thin black ring, B' - thin black ring, thick black ring and black hole, C' - black hole.

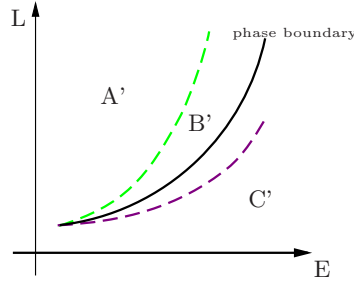


Figure 11: Existence regions and phase boundary for black holes / rings.

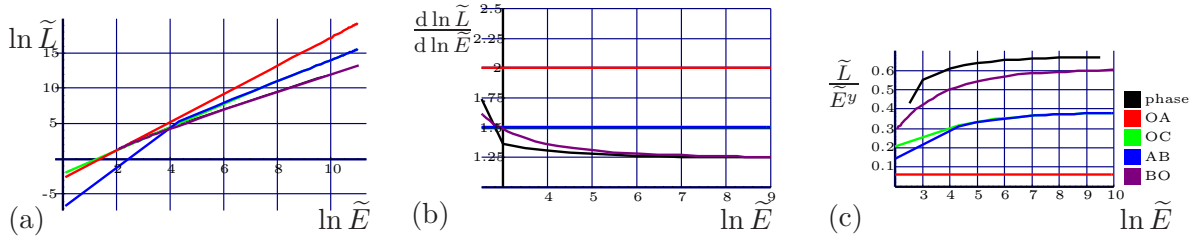


Figure 12: (a) log-log plots of the boundaries, (b) gradients of log-log plots, (c) $\tilde{L}/\tilde{E}^y \rightarrow x$.

1).

It is meaningless to compare the x 's directly, as they are dimensionful quantities. However, when two y 's have the same value, the ratio of the corresponding x 's is dimensionless and may be compared. For black rings $x_{AB} = \sqrt{32G/27\pi}$, $x_{BO} = \sqrt{G/\pi}$ and $x_{phase} = \sqrt{256G/243\pi}$, so $x_{AB}/x_{OC} = 1$, $x_{OC}/x_{BO} = \sqrt{32/27}$ and $x_{BO}/x_{phase} = 9\sqrt{3}/16$. For plasmaballs and plasmaring, if we used the dimensionless quantities (41), we find $x_{OA} = \frac{1}{16}$, $x_{AB} = x_{OC} = 2/3^{3/2}$, $x_{BO} \approx 0.60$ and $x_{phase} \approx 0.67$. Therefore $x_{AB}/x_{OC} = 1$ and $x_{BO}/x_{phase} \approx 0.91$.

This is summarised in table 1. Note that the extremality boundaries, OA, AB and OC, occur precisely where at least one of the approximations discussed in §5.2 breaks down. Therefore, nothing quantitative about these boundaries should be trusted.

5.5 Turning point stability

We have seen in §5.3 that the spinning plasma solution of maximal entropy is the plasmaball (at low angular momentum) or the large plasmaring (at high angular momentum). The 'phase transition' between these two solutions may be thought of as being of first order (in the sense that the two competing solutions are different at the phase transition point). The small plasmaring is entropically subdominant to both the plasmaball and the large

Quantity	Black rings	Plasmarings
y_{OA}	N/A	2
y_{AB}	3/2	3/2
y_{OC}	3/2	3/2
y_{BO}	3/2	1.25
y_{phase}	3/2	1.25
x_{AB}/x_{OC}	1	1
x_{OC}/x_{BO}	$\sqrt{32/27}$	N/A
x_{BO}/x_{phase}	$9\sqrt{3}/16 \approx 0.97$	0.91

Table 1: Comparison of scalings of boundaries for black rings and plasmarings.

plasmaring whenever it exists.

This situation appears to lend itself to a description in terms of a Landau diagram, with the entropy given by a function of the (unidentified) order parameter that has two maxima (the plasmaball and the large plasmaring) separated by a single minimum (the small plasmaring). This analogy suggests - and we conjecture that - the small plasmaring is always dynamically unstable, while the plasmaball and large plasmarings are dynamically stable with respect to axisymmetric fluctuations.

An honest verification of our conjecture would require a study of the spectrum of linear fluctuations about our plasmaball and plasmaring solutions, an analysis that we have not carried out. In this subsection, however, we present some evidence for our conjecture, using the ‘turning point’ stability analysis of [12] (see [13] for discussion and references).

Consider a (not necessarily stable) equilibrium configuration that changes from being stable to unstable under continuous variation. The configurations we apply these considerations to are plasmarings; according to our conjecture these rings are stable to axisymmetric fluctuations when large but become unstable to the same modes when small. At the boundary of stability, the matrix of second derivatives of the entropy with respect to off shell variations (or ‘order parameters’) of the configuration under question develops a zero eigenvalue. In the neighbourhood of this special point, a small change in the thermodynamic potentials of the solution give rise to a large change in the order parameter along the zero eigenvalue direction (as such a change is entropically inexpensive). As argued in [14–17], this results in a divergent contribution to the second derivative of the equilibrium entropy as a function of equilibrium thermodynamic quantities (for instance the angular momentum at fixed energy) proportional to the negative inverse of the small eigenvalue.

It follows that a configuration that changes stability has divergent second derivatives of entropy with respect to - say - angular momentum. Moreover the sign of this second derivative is positive in the ‘more stable’ phase and negative in the ‘less stable’ phase. Note that the turning point method gives information about the change in the number of unstable directions about a solution, but does not yield information about the absolute

number of instabilities.¹¹

The turning point method is useful because it yields information about stability properties, with respect to off shell fluctuations, of phases, using information only about on shell variations. It is especially useful in the study of nonextensive systems like black holes, for which negative specific heats do not necessarily imply dynamical instability (note that we're working with the microcanonical ensemble, unlike the grand-canonical considerations of [18]). This method has been used to study the stability of black rings in 5 dimensions [13, 19]; it suggests that small black rings are always unstable, while large black rings are more stable in that context. This result corroborates the explicit linear fluctuation analysis about the flat space black rings [10].

We now proceed to apply the turning point method to our plasmarings. Define

$$\beta = \left(\frac{\partial \tilde{S}}{\partial \tilde{E}} \right)_{\tilde{L}} = \frac{1}{\tilde{T}} = \frac{1}{[g_+(v_o, \tilde{\omega})]^{1/4}}, \quad (56)$$

$$\psi = \left(\frac{\partial \tilde{S}}{\partial \tilde{L}} \right)_{\tilde{E}} = -\frac{\tilde{\Omega}}{\tilde{T}} = -\frac{\tilde{\omega}}{[g_+(v_o, \tilde{\omega})]^{1/4}}. \quad (57)$$

In fig.13 we have plotted ψ against angular momentum at fixed energy for our ring solutions. This graph has a single turning point, precisely at the point at which the large ring turns into a small ring. The slope of the curve turns from positive (for the large ring) to negative (for the small ring) in upon passing through the turning point, consistent with our conjecture about the stability properties of plasmarings. More generally, fig.13 is qualitatively similar to the equivalent graph of [13, fig.6(b)] for black hole and black rings in flat 5 dimensional space, except that the large black ring curves back down as we increase \tilde{L} . This difference has no impact on stability analysis, as the turning point method links instabilities to vertical tangents rather than horizontal tangents (even though a heat capacity/susceptibility changes sign as one crosses a horizontal tangent).

In conclusion, the turning point method indicates that the small ring has an additional instability as compared to the large ring. Note that it is perfectly possible that both the large and the small ring are unstable, for example to fluctuations that break rotational symmetry.

6 Four dimensional plasmarings

In the rest of this paper we turn to a consideration of localised plasma configurations in certain massive 4 and 5 dimensional field theories obtained by compactifying related 5 and 6 dimensional CFTs on a Scherk-Schwarz circle. Although the field theories in

¹¹Moreover, this method only links vertical tangents - and not vertical asymptotes - in the graph of the first derivative of entropy with respect to (say) angular momentum vs. angular momentum (a conjugacy diagram) to instabilities, as vertical asymptotes occur at boundaries of equilibrium solution space instead of separating solutions of differing degrees of stability.

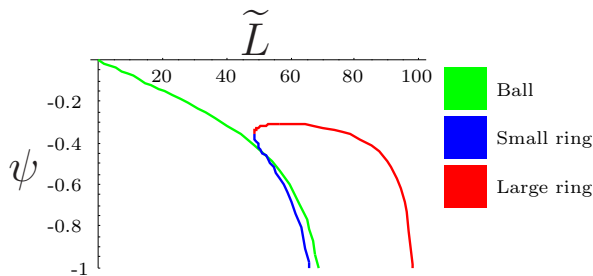


Figure 13: Conjugacy diagram: ψ as a function of angular momentum, \tilde{L} for fixed energy, $\tilde{E} = 40$.

question are not gauge theories (e.g. the 5 dimensional massive theory could be obtained by compactifying the (0,2) theory on the world volume of an M5 brane on a Scherk-Schwarz circle) they undergo first order ‘deconfining’ transitions and the high temperature phase of these theories admits a fluid dynamical description. The fluid configurations we will construct are dual to localised black holes and black rings in Scherk-Schwarz compactified AdS_6 and AdS_7 respectively.

In this section we study stationary solutions of fluid dynamics in 3+1 dimensional field theories. Our study will be less thorough than our 3 dimensional analysis above; we find solutions analogous to those in 3 dimensions, but we postpone the complete parameterisation and study of the thermodynamic properties of these solutions to future work. In Appendix A we have derived the equations relevant to stationary fluid flow in 5 dimensions, but we leave the study of their solutions (and their higher dimensional counterparts) to future work.

6.1 Stress tensor and equations of motion

In this section we set up the equations of motion of our fluid. We proceed in direct imitation of our analysis of $d = 3$ above. We use the metric

$$ds^2 = -dt^2 + dr^2 + r^2 d\phi^2 + dz^2. \quad (58)$$

This gives the same non-zero Christoffel symbols as before (19). We choose the origin so that $r = 0$ is the axis of rotation and there is a reflection symmetry in the plane $z = 0$.

For our configurations, $u^\mu = \gamma(1, 0, \omega, 0)$ with $\gamma = (1 - \omega^2 r^2)^{-1/2}$. We assume that the surface can be described by $f(r, z) = z - h(r)$. In the interior of the fluid, This leads to the stress tensor

$$T_{\text{perfect}}^{\mu\nu} = \begin{pmatrix} \gamma^2(\rho + \omega^2 r^2 P) & 0 & \gamma^2 \omega(\rho + P) & 0 \\ 0 & P & 0 & 0 \\ \gamma^2 \omega(\rho + P) & 0 & \frac{\gamma^2}{r^2}(\omega^2 r^2 \rho + P) & 0 \\ 0 & 0 & 0 & P \end{pmatrix} \quad (59)$$

and the surface stress tensor

$$T_{\text{surface}}^{\mu\nu} = \frac{\sigma\delta(z-h(r))}{\sqrt{1+h'(r)^2}} \begin{pmatrix} 1+h'(r)^2 & 0 & 0 & 0 \\ 0 & -1 & 0 & -h'(r) \\ 0 & 0 & -\frac{1+h'(r)^2}{r^2} & 0 \\ 0 & -h'(r) & 0 & -h'(r)^2 \end{pmatrix} \quad (60)$$

Just as in $d = 3$, the only potentially nonzero term in $T_{\text{dissipative}}^{\mu\nu}$ is proportional to $\frac{d}{dr} \left[\frac{T}{\gamma} \right]$. As in $d = 3$, it will turn out that this quantity vanishes on our solutions, so we simply proceed setting $T_{\text{dissipative}}^{\mu\nu}$ to zero.

The equations of motion, $\nabla_{\mu} T^{\mu\nu} = 0$, reduce to

$$\begin{aligned} 0 &= \frac{\partial P}{\partial r} - \frac{\omega^2 r}{1 - \omega^2 r^2} (\rho + P) \mp 2\sigma H h'(r) \delta(z - h(r)), \\ 0 &= \frac{\partial P}{\partial z} \pm 2\sigma H \delta(z - h(r)), \end{aligned} \quad (61)$$

where the upper sign refers to the upper ($z > 0$) surface and

$$H = \mp \frac{r h'' + h'(1 + h'^2)}{2r(1 + h'^2)^{3/2}} \quad (62)$$

is the mean curvature of the surface [20].

6.2 Solutions

Our analysis so far has been rather general; to proceed further we use the equations of state (14). We define dimensionless variables as before

$$\tilde{\omega} = \frac{\sigma\omega}{\rho_0}, \quad v = \omega r, \quad \tilde{h}(v) = \omega h(r). \quad (63)$$

Using the equation of state (14), we can rewrite (61) in the bulkinterior of the fluid as

$$\begin{aligned} \frac{1}{\rho - \rho_0} \frac{d\rho}{dv} &= \frac{5v}{1 - v^2}, \\ \implies (\rho(v) - \rho_0) (1 - v^2)^{5/2} &= 4K\rho_0, \end{aligned} \quad (64)$$

where K is an integration constant. This means that the pressure and temperature are

$$P = \rho_0 \left(\frac{K}{(1 - v^2)^{5/2}} - 1 \right), \quad T = \gamma \left(\frac{K\rho_0}{\alpha} \right)^{1/5}, \quad (65)$$

(notice that this justifies our neglect of heat flow).

Integrating (61) across an outer surface gives

$$P = 2\sigma H \quad \text{or} \quad \frac{K}{(1-v^2)^{5/2}} - 1 = -\tilde{\omega} \frac{v\tilde{h}'' + \tilde{h}'(1 + \tilde{h}'^2)}{v(1 + \tilde{h}'^2)^{3/2}}. \quad (66)$$

This can be integrated once to give

$$\frac{v\tilde{h}'}{\sqrt{1 + \tilde{h}'^2}} = -\frac{K}{3\tilde{\omega}(1-v^2)^{3/2}} + \frac{v^2}{2\tilde{\omega}} + \frac{C}{\tilde{\omega}}, \quad (67)$$

where C is another integration constant.

If we introduce a parameter l equal to the distance along the surface, measured from $(v, \tilde{h}) = (v_o, 0)$, we have $\frac{dl}{dv} = -\sqrt{1 + \tilde{h}'^2}$. Then (67) can be written as

$$\begin{aligned} \frac{d\tilde{h}}{dl} &= \frac{2K - 3(v^2 + 2C)(1-v^2)^{3/2}}{6\tilde{\omega}v(1-v^2)^{3/2}}, \\ \frac{dv}{dl} &= -\frac{\sqrt{36\tilde{\omega}^2v^2(1-v^2)^3 - [2K - 3(v^2 + 2C)(1-v^2)^{3/2}]^2}}{6\tilde{\omega}v(1-v^2)^{3/2}}, \\ \frac{d\tilde{h}}{dv} &= -\frac{2K - 3(v^2 + 2C)(1-v^2)^{3/2}}{\sqrt{36\tilde{\omega}^2v^2(1-v^2)^3 - [2K - 3(v^2 + 2C)(1-v^2)^{3/2}]^2}}. \end{aligned} \quad (68)$$

It follows that the outer surface of our plasma configuration is given by

$$\tilde{h}(v) = \int_{v_o}^v dx \left(-\frac{2K - 3(x^2 + 2C)(1-x^2)^{3/2}}{\sqrt{36\tilde{\omega}^2x^2(1-x^2)^3 - [2K - 3(x^2 + 2C)(1-x^2)^{3/2}]^2}} \right) \quad (69)$$

Of course this only makes sense provided

$$6\tilde{\omega}x(1-x^2)^{3/2} \geq |2K - 3(x^2 + 2C)(1-x^2)^{3/2}| \quad \forall x \in (v, v_o). \quad (70)$$

Note also the conditions $\rho > \rho_0 \implies K > 0$ and, of course, $0 < v_i < v_o$.

Inner boundaries to the plasma configuration (if they exist) obey the equation $P = -2\sigma H$. The equivalent of (68), with a new integration constant D replacing C (the integration constant K is a property of the plasma, not the surfaces), is

$$\begin{aligned} \frac{d\tilde{h}}{dl} &= -\frac{2K - 3(v^2 + 2D)(1-v^2)^{3/2}}{6\tilde{\omega}v(1-v^2)^{3/2}}, \\ \frac{dv}{dl} &= -\frac{\sqrt{36\tilde{\omega}^2v^2(1-v^2)^3 - [2K - 3(v^2 + 2D)(1-v^2)^{3/2}]^2}}{6\tilde{\omega}v(1-v^2)^{3/2}}, \\ \frac{d\tilde{h}}{dv} &= \frac{2K - 3(v^2 + 2D)(1-v^2)^{3/2}}{\sqrt{36\tilde{\omega}^2v^2(1-v^2)^3 - [2K - 3(v^2 + 2D)(1-v^2)^{3/2}]^2}}. \end{aligned} \quad (71)$$

Horizon topology	Plasma topology	Object
S^4	B^3	Ball
$S^3 \times S^1$	$B^2 \times S^1$	Ring
$S^2 \times S^2$	$B^1 \times S^2$	Hollow ball
$S^2 \times S^1 \times S^1$	$B^1 \times S^1 \times S^1$	Hollow ring
$S^1 \times S^1 \times S^1 \times S^1$	None	None

Table 2: Topologies of gravity and plasma solutions

The profiles of such boundaries may be obtained by integrating the equation above.

Even before doing any analysis, we will find it useful to give names to several easily visualised, topologically distinct fluid configurations.

Ordinary ball: $v'(l) = \tilde{h}(l) = 0$ at $v = v_o$. $\tilde{h}'(l) > 0$ for $0 < v < v_o$. $\tilde{h}'(l) = 0$ at $v = 0$.

Pinched ball: $v'(l) = \tilde{h}(l) = 0$ at $v = v_o$. $\tilde{h}'(l) > 0$ for $0 < v < v_m$. $\tilde{h}'(l) = 0$ at $v = v_m$. $\tilde{h}'(l) < 0$ for $0 < v < v_m$. $\tilde{h}'(l) = 0$ at $v = 0$.¹²

Ring: $v'(l) = \tilde{h}(l) = 0$ at $v = v_o$. $\tilde{h}'(l) > 0$ for $v_m < v < v_o$. $\tilde{h}'(l) = 0$ at $v = v_m$. $\tilde{h}'(l) < 0$ for $v_i < v < v_m$. $v'(l) = \tilde{h}(l) = 0$ at $v = v_i$, where $v_i < v_m < v_o$.

Examples of these surfaces can be seen in figs.16-17. Each of these solutions could have lumps of fluid eaten out of them. We will use the terms

Hollow ball: A ball (pinched or ordinary) with a ball cut out from its inside.

Hollow ring: A ring with a ring cut out from its inside.

Toroidally hollowed ball: A ball with a ring cut out from its inside.

It is easy to work out the horizon topology of the gravitational solutions dual to the plasma topologies listed above. [22] have obtained a restriction on the topologies of horizons of stationary black holes in any theory of gravity that obeys the dominant energy condition; any product of spheres obeys the conditions from their analysis. Although the dominant energy condition is violated in AdS space, in table 2, we have listed all 4 dimensional horizons that are topologically products of lower dimensional spheres, and note that all but one of these configurations is obtained from the dual to plasma objects named above (B^3 is a ball, B^2 is a disc and B^1 is an interval). The last one, $T^4 = S^1 \times S^1 \times S^1 \times S^1$, is a marginal case of the theorem.

In the rest of this section we will determine all stationary, rigidly spinning solutions of the equations of fluid dynamics described above.

¹²Black holes with wavy horizons in six dimensions and above were predicted in [21].

6.2.1 Ordinary ball

We search for solutions of (69) for which $\tilde{h}'(v)$ vanishes at $v = 0$ and blows up at the outermost point of the surface v_0 ; we also require that \tilde{h} decrease monotonically from 0 to v_0 . The first condition sets $K = 3C$. The condition that $v'(l)$ is zero at v_0 may be used to determine $\tilde{\omega}$ as a function of v_0 and K from the linear equation

$$2K - (3v_0^2 + 2K)(1 - v_0^2)^{3/2} = 6\tilde{\omega}v_0(1 - v_0^2)^{3/2}, \quad (72)$$

(the choice of positive square root comes from the fact that the LHS above is positive).

Note that the numerator of the formula for $\tilde{h}'(v)$ be written as

$$2 \left[1 - (1 - v^2)^{3/2} \right] \left(K - \frac{3v^2(1 - v^2)^{3/2}}{2 \left[1 - (1 - v^2)^{3/2} \right]} \right)$$

and $2 \left(1 - (1 - v^2)^{3/2} \right) \geq 3v^2(1 - v^2)^{3/2}$. Thus, $K > 1$ guarantees our monotonicity requirement. From (65), we see that this also ensures that the pressure is positive throughout the ball.

In summary, the full set of ordinary ball solution is obtained by substituting $C = K/3$ and $\omega = \omega(K, v_0)$ (obtained by solving (72)) into (69). This procedure gives us a ball solution for any choice of $K > 1$ and $v_0 > 0$.

In figs.16,17 we present a plot of the profile $\tilde{h}(v)$ for the ball solution at $v_0 = 0.8$, $K = 1.5$.

6.2.2 Pinched ball

The pinched ball satisfies all the conditions of the ordinary ball except for the monotonicity requirement on $\tilde{h}(v)$; in fact the function $\tilde{h}(v)$ is required to first increase and then decrease as v runs from 0 to v_0 . It follows that C and $\tilde{\omega}$ for these solutions are determined as in the previous subsection ($C = K/3$ and ω from (72)) however the requirement $\tilde{h}''(v) > 0$ at $v = 0$ forces $K < 1$. This ensures that $\tilde{h}'(v) > 0$ at small v and $\tilde{h}'(v) < 0$ at larger v . It also ensures that the solution has negative pressure at the origin and positive pressure at the outermost radius.

Not every choice of $(K, v_0) \in [0, 1]$, however, yields an acceptable pinched ball solution. As we decrease v_0 from 1, at fixed K , it turns out that $\tilde{h}(0)$ decreases, and in fact vanishes at a critical value of v_0 . Solutions at smaller v_0 are unphysical. The physical domain, in (K, v_0) space is given by the inequality

$$\Delta\tilde{h} \equiv - \int_0^{v_0} \frac{d\tilde{h}}{dv} dv = \int_0^{v_0} \frac{2K - (3v^2 + 2K)(1 - v^2)^{3/2}}{\sqrt{36\tilde{\omega}^2 v^2 (1 - v^2)^3 - [2K - (3v^2 + 2K)(1 - v^2)^{3/2}]^2}} dv \geq 0. \quad (73)$$

We should also ensure that (70) is not violated, i.e.

$$Q(v_0, K) \equiv \inf_{v \in (0, v_0)} \left\{ 36\tilde{\omega}^2 v^2 (1 - v^2)^3 - [2K - (3v^2 + 2K)(1 - v^2)^{3/2}]^2 \right\} \geq 0. \quad (74)$$

The boundary of the domain permitted by (73) is plotted in fig.14. We have also plotted the boundary of the region where (74) is violated. We see that (73) is the stricter constraint, and that (74) is not violated for ordinary balls either. The full set of pinched ball solutions is parameterised by values of v_o and K in the region indicated in fig.14.

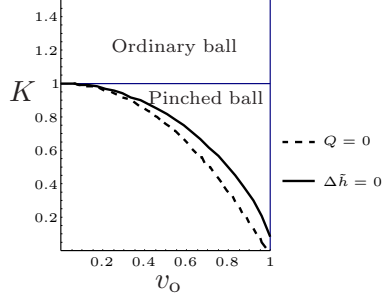


Figure 14: Domain of ball solutions.

In figs.16,17 we present an example of the profile $\tilde{h}(v)$ for the pinched ball solution at parameters $v_o = 0.8$, $K = 0.55$.

6.2.3 Ring

The plasma of the ring configuration excludes the region $v < v_i$; as this region omits $v = 0$, K and C are not constrained as before.

As $v'(l)$ vanishes at v_i, v_o we have the following constraints

$$\begin{aligned} 2K - 3(v_i^2 + 2C)(1 - v_i^2)^{3/2} &= -6\tilde{\omega}v_i(1 - v_i^2)^{3/2}, \\ 2K - 3(v_o^2 + 2C)(1 - v_o^2)^{3/2} &= 6\tilde{\omega}v_o(1 - v_o^2)^{3/2}. \end{aligned} \quad (75)$$

the choice of negative/positive square roots comes from the requirements that $\tilde{h}'(l) < 0$ at $v = v_i$ and $\tilde{h}'(l) > 0$ at $v = v_o$. These equations may be used to solve for C and $\tilde{\omega}$ as a function of K, v_i, v_o . $K(v_o, v_i)$ may then be determined from the requirement that $\tilde{h}(v_i) = \tilde{h}(v_o) = 0$, i.e.

$$\int_{v_i}^{v_o} \frac{d\tilde{h}}{dv} dv = - \int_{v_i}^{v_o} \frac{2K - 3(v^2 + 2C)(1 - v^2)^{3/2}}{\sqrt{36\tilde{\omega}^2 v^2 (1 - v^2)^3 - [2K - 3(v^2 + 2C)(1 - v^2)^{3/2}]^2}} dv = 0. \quad (76)$$

In practice, it is easier to first eliminate K and C using (75), then substitute $v_i = \tilde{\omega}\tilde{r}_i$, $v_o = \tilde{\omega}\tilde{r}_o$ and use (76) to solve for $\tilde{\omega}$ at fixed \tilde{r}_i and \tilde{r}_o . after this, one can determine K, v_i and v_o from $\tilde{\omega}, \tilde{r}_i$ and \tilde{r}_o . We present a 3 dimensional plot of K as a function of v_i and v_o for $1 < \tilde{r}_o < 10$, $0.1 < \tilde{r}_i/\tilde{r}_o < 0.9$ in fig.15. All of these solutions have $K > 0$, as required. Unfortunately, with this method, one cannot see if there is a physically acceptable solution for the whole range of $0 < v_i < v_o < 1$. It appears that there is a solution for every value of $\tilde{r}_i < \tilde{r}_o$.

In figs.16,17 we plot the profile function $\tilde{h}(v)$ for the ring solution at parameters $\tilde{r}_i = 10$, $\tilde{r}_o = 20$.

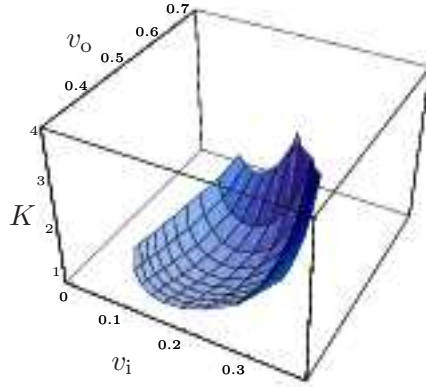


Figure 15: K as a function of v_i and v_o for ring solutions.

6.2.4 Hollow ball

In this subsection we will demonstrate the non-existence of rigidly rotating hollow ball solutions to the equations of fluid dynamics. Let us suppose such a solution did exist. The inner surface must have vanishing gradient at $v = 0$; this sets $D = K/3$. Now let the outermost point of the eaten out region be $v = \tilde{v}_o$. The inner surface must have a vertical tangent at \tilde{v}_o . This also implies that the outer surface also has a vertical tangent at \tilde{v}_o (the condition for a vertical tangent is identical for an outer or inner surface). However, such points saturate the inequality (70) and, as discussed in §§6.2.2, this never happens in the interior of a ball. It follows that hollow ball solutions do not exist.

6.2.5 Hollow ring and toroidally hollowed ball

Let us first consider the possibility of the existence of a toroidally hollowed ball solution. Let the innermost and outermost part of the hollowed out region occur at $v = \tilde{v}_i$ and $v = \tilde{v}_o$ respectively. Let us define $a(v) = 6\tilde{\omega}v(1 - v^2)^{3/2}$ and $b(v) = -2K + 3(v^2 + 2D)(1 - v^2)^{3/2}$ where D is the integration constant for the hollow. From (71) it must be that

$$a(\tilde{v}_o) = b(\tilde{v}_o) \quad a(\tilde{v}_i) = -b(\tilde{v}_i) \quad |b(v)| < |a(v)| \quad \forall v \in (\tilde{v}_i, \tilde{v}_o)$$

For these conditions to apply, $b(v)$ must start out negative at $v = \tilde{v}_i$, increase, turn positive, and cut the $a(v)$ curve from below at $v = \tilde{v}_o$. We have performed a rough numerical scan of allowed values of parameters $(K, \tilde{\omega}, D)$; it appears that this behaviour never occurs (although we do not, however, have a rigorous proof for this claim). For all physically acceptable values of parameters, the curve $b(v)$ appears to either stay entirely below $a(v)$ or to cut it from above.¹³

¹³We emphasise that this behaviour appears to be true only for $\tilde{\omega} > \tilde{\omega}_{min}(K)$ where $\tilde{\omega}_{min}(K)$ is the smallest allowed value of $\tilde{\omega}$ at fixed K (see fig.14). It is easy to arrange for $b(v)$ to cut $a(v)$ from below when $\tilde{\omega}$ is taken to be arbitrarily small at fixed K and D , but this is unphysical.

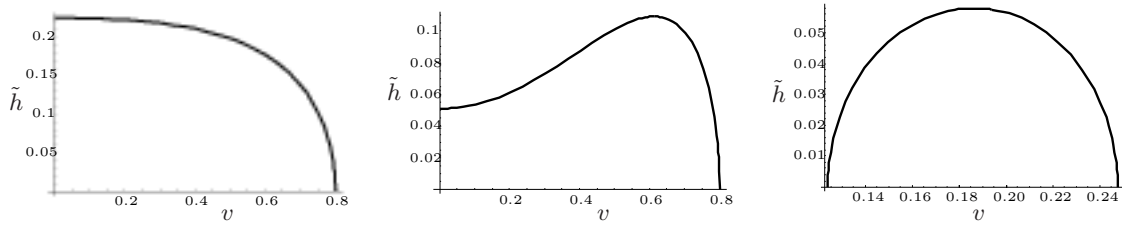


Figure 16: Profile of the surface of an ordinary ball, pinched ball and ring.

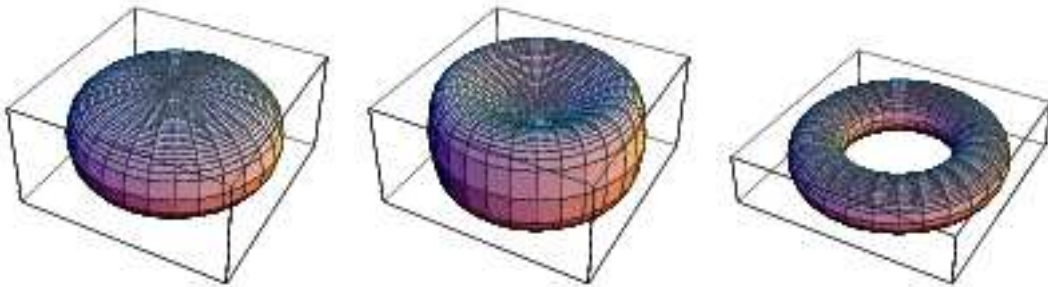


Figure 17: 3D plot of the surface of an ordinary ball, pinched ball and ring.

These considerations, which could presumably be converted into a proof with enough effort, lead us to believe that the existence of hollow balls is highly unlikely. We believe that similar reasoning is likely to rule out the existence of hollow rings, although this is more difficult to explicitly verify, as our understanding of the parameter ranges for acceptable ring solutions is incomplete.

In order to understand intuitively why hollow rings and toroidally hollow balls are unlikely, note that the pressure at the inner and outermost parts of the hollowed out region is given by

$$P(\tilde{v}_i) = \rho_0 \tilde{\omega} \left(-|v''_{v=\tilde{v}_i}| + \frac{1}{\tilde{v}_i} \right), \quad P(\tilde{v}_o) = \rho_0 \tilde{\omega} \left(-|v''_{v=\tilde{v}_o}| - \frac{1}{\tilde{v}_o} \right),$$

where $v''_{v=\tilde{v}_i}$ is positive and $v''_{v=\tilde{v}_o}$ is negative. Provided that $|v''_{v=\tilde{v}_i}|$ and $|v''_{v=\tilde{v}_o}|$ are not drastically different, we would require $P(\tilde{v}_i) > P(\tilde{v}_o)$. However, the pressure increases monotonically with radius.

In conclusion, we strongly suspect, but have not yet fully proved, that the full set of rigidly rotating solutions to the equations of fluid dynamics in $d = 4$ is exhausted by ordinary balls, pinched balls and rings.

7 Discussion

In this paper we have emphasised that the AdS/CFT correspondence implies a duality between nonsingular classical gravitational solutions with horizons, and solutions to the boundary equations of fluid dynamics. This connection has previously been utilised by several authors to obtain gravitational predictions for various fluid viscosities and conductivities (see, for instance, [3] and references therein). The new element in our work is the incorporation of boundaries separating the fluid from the vacuum into the Navier-Stokes equations. This feature (which relies on the explicit gravitational construction of the domain wall in [2]) allowed us to study stationary *finite energy* lumps of plasma, which are dual to localised black holes and black rings in the bulk.

All our work (and easily imagined generalisations) apply to confining field theories. Stationary black holes in such backgrounds sit at the IR ends of the geometry; the boundary shadow of such black holes is a lump of deconfined fluid of size $R + \mathcal{O}(\Lambda_{\text{gap}}^{-1})$. The fluid dynamic equations accurately describe such lumps only when $R \gg \Lambda_{\text{gap}}^{-1}$, in the same limit the fluid yields an approximately local representation of the horizon. Consequently, the AdS/CFT correspondence provides an approximately local fluid description of horizon dynamics in the long wavelength limit. This result is strongly reminiscent of the Membrane paradigm of black hole physics [5, 23, 24], and may constitute the precise version of this idea in the context of asymptotically AdS spaces.

All the specific results of this paper are based on the equations of state (14), which are valid for the high temperature phase of Scherk-Schwarz compactified conformal field theories (dual to gravity in Scherk-Schwarz compactified AdS space). However the only qualitative feature of this equation of state that was important for the existence of the solutions of this paper is that the fluid pressure vanishes at finite energy density. In fig.9 we have plotted the maximum and minimum values of $\ln \mathcal{T}/\mathcal{T}_c$ in our solutions, as a function of energy and angular momentum. Note that at large values of charges (and away from extremality bounds) each of these quantities tends to zero. This demonstrates that over large classes of our solutions, the fluid temperature is always close to the phase transition temperature. As a consequence such solutions ‘sample’ only the fluid equation of state only in the neighbourhood around the zero pressure point, and so would exist in any fluid whose pressure vanishes at finite energy density.

Our results suggest several directions for future research. It would be interesting to analyse the stability of small fluctuations about the solutions presented in this paper. As we have mentioned in §5.5, we expect the small ring to be unstable to axisymmetric fluid fluctuations, while we expect the ball and the large ring to be stable to such fluctuations. However, it is quite possible that such an analysis would reveal that the large ring solutions of this paper have a Plateau-Rayleigh type instability that maps to Gregory-Laflamme instabilities (see also [4])¹⁴ of the dual bulk solutions.

Although we have not mentioned this in the text, there exists a scaling limit in which

¹⁴We thank T. Wiseman for suggesting this.

the thin plasmaring solutions simplify greatly.¹⁵ In this limit ($\tilde{\omega} \rightarrow 0$ with v_i fixed), the 3D plasmaring reduces to a straight strip of moving fluid. The fluid pressure vanishes on this strip, and the fluid velocity is constant across the strip (more precisely $v_o = v_i + \frac{1-v_i^2}{2v_i^2}\tilde{\omega} + \mathcal{O}(\tilde{\omega}^2)$ so that $\tilde{r}_o - \tilde{r}_i = \frac{1-v_i^2}{2v_i^2} + \mathcal{O}(\tilde{\omega})$). Similarly, there should exist scaling limit under which the 4 dimensional plasmaring reduces to an infinite stationary cylinder, with fluid flow along the axis. Various dynamical properties of large rings (e.g. the potential Gregory-Laflamme type instability alluded to in the previous paragraph) will probably prove easiest to study in this scaling limit.

It should also be relatively straightforward, and rather interesting, to more fully analyse the thermodynamics of the four dimensional solutions presented in this paper. This thermodynamics may have interesting features; for example, it has been suggested that ultra-spinning black holes in six dimensional flat space are unstable [21] and it would be interesting to see if the same is true of our (pinched?) plasmaballs.

An extension of our work to obtain the moduli space of five and higher dimensional fluid configurations - and so seven and higher dimensional gravitational black solutions should also be possible (though analytic solutions may be harder to obtain in higher dimensions). Such an extension would yield interesting information about horizon topologies in higher dimensional gravitational theories. An obvious conjecture based on intuition from fluid flows would be that the full set of stationary fluid solutions in five dimensions appear in three distinct topological classes; solutions whose bulk dual topologies would be S^5 , $S^4 \times S^1$ and $S^3 \times S^1 \times S^1$. The reason one might expect the last solution is that in five (but no lower) dimensions, it is possible to have solutions that rotate about two independent axes; these two rotations should be able to create their own distinct centrifugal ‘holes’, resulting in the above topology. It would be very interesting to check whether this conjecture is borne out.

Acknowledgements

We would like to thank D. Astefanesei, I. Bena, K. Damle, R. Emparan, R. Gopakumar, R. Jena, S. Raju and S. Wadia for useful conversations. We would especially like to thank O. Aharony and T. Wiseman for useful comments. The work of S.M. was supported in part by a Swarnajayanti Fellowship. We must also acknowledge our debt to the steady and generous support of the people of India for research in basic sciences.

¹⁵We thank T. Wiseman again for pointing this out to us.

Appendices

A Five dimensional plasmarrings

In the bulk of this paper we have presented an analysis of stationary fluid configurations of the three and four dimensional fluid flows. The analysis of analogous configurations in one higher dimension has an interesting new element. The rotation group in four spatial dimensions, $SO(4)$, has rank 2. Consequently a rotating lump of fluid in five dimensions will be characterised by three rather than two conserved charges (two angular momenta plus energy). When one of the two angular momenta is set to zero, it seems likely that the set of stationary solutions will be similar to those of the four dimensional fluid; in this limit we expect ball and ring configurations whose dual bulk horizon topologies are S^5 and $S^4 \times S^1$ respectively. However turning on the second angular momentum on the ring solution could centrifugally repel the fluid away from the second rotational axis, leading to a fluid configuration with dual bulk horizon topology $S^1 \times S^1 \times S^3$. Such configurations have not yet been discovered in gravity, and it would be exciting to either construct them in fluid mechanics, or to rule out their existence.

In this appendix we set up and partially solve the equations of stationary fluid flow in five dimensions. While the stationary equations of fluid dynamics are trivial to solve in the bulk in every dimension, boundary conditions are harder to impose in higher dimensions. In the particular case of 5 dimensions, the imposition of these boundary conditions requires the solution of a 2nd order ordinary differential equation, that we have not (yet?) been able to solve. It may be that a full study of this case would require careful numerical analysis, which we leave to future work. In the rest of this appendix we simply set up the relevant equations, and comment on the dual bulk interpretations of various possible solutions.

Consider a fluid propagating in flat five dimensional space

$$ds^2 = -dt^2 + dr_1^2 + r_1^2 d\phi_1^2 + dr_2^2 + r_2^2 d\phi_2^2.$$

Consider a fluid flow with velocities given by $u^\mu = \gamma(1, 0, \omega_1, 0, \omega_2)$, where $\gamma = (1 - v_1^2 - v_2^2)^{-1/2}$, $v_1 = \omega_1 r_1$ and $v_2 = \omega_2 r_2$. Let the fluid surface be given by $f(r_1, r_2) = r_2 - h(r_1) = 0$.

The stress tensor evaluated on such a fluid configuration is given by

$$T_{\text{perfect}}^{\mu\nu} = \begin{pmatrix} \gamma^2(\rho + (v_1^2 + v_2^2)P) & 0 & \gamma^2\omega_1(\rho + P) & 0 & \gamma^2\omega_2(\rho + P) \\ 0 & P & 0 & 0 & 0 \\ \gamma^2\omega_1(\rho + P) & 0 & \frac{\gamma^2}{r_1^2}(v_1^2\rho + (1 - v_2^2)P) & 0 & \gamma^2\omega_1\omega_2(\rho + P) \\ 0 & 0 & 0 & P & 0 \\ \gamma^2\omega_2(\rho + P) & 0 & \gamma^2\omega_1\omega_2(\rho + P) & 0 & \frac{\gamma^2}{r_2^2}(v_2^2\rho + (1 - v_1^2)P) \end{pmatrix}$$

$$T_{\text{dissipative}}^{\mu\nu} = -\kappa\gamma^2 \begin{pmatrix} 0 & \partial_{r_1} & 0 & \partial_{r_2} & 0 \\ \partial_{r_1} & 0 & \omega_1\partial_{r_1} & 0 & \omega_2\partial_{r_1} \\ 0 & \omega_1\partial_{r_1} & 0 & \omega_1\partial_{r_2} & 0 \\ \partial_{r_2} & 0 & \omega_1\partial_{r_2} & 0 & \omega_2\partial_{r_2} \\ 0 & \omega_2\partial_{r_1} & 0 & \omega_2\partial_{r_2} & 0 \end{pmatrix} \frac{\mathcal{T}}{\gamma}$$

$$T_{\text{surface}}^{\mu\nu} = \frac{\sigma\delta(r_2 - h(r_1))}{\sqrt{1 + h'^2}} \begin{pmatrix} 1 + h'^2 & 0 & 0 & 0 & 0 \\ 0 & -1 & 0 & -h' & 0 \\ 0 & 0 & -\frac{1+h'^2}{r_1^2} & 0 & 0 \\ 0 & -h' & 0 & -h'^2 & 0 \\ 0 & 0 & 0 & 0 & -\frac{1+h'^2}{r_2^2} \end{pmatrix}$$

As usual, we will temporarily ignore $T_{\text{dissipative}}^{\mu\nu}$, justifying this when we find that $\mathcal{T} \propto \gamma$. The nontrivial equations of motion that follow from (5) take the form

$$\begin{aligned} 0 &= \nabla_{\mu} T^{\mu r_1} = \partial_{r_1} P - \gamma^2 \omega_1^2 r_1 (\rho + P) - \sigma G h'(r_1) \delta(r_2 - h(r_1)) \\ 0 &= \nabla_{\mu} T^{\mu r_2} = \partial_{r_2} P - \gamma^2 \omega_2^2 r_2 (\rho + P) + \sigma G \delta(r_2 - h(r_1)) \end{aligned} \quad (77)$$

where

$$G = -\frac{r_1 h h'' + (1 + h'^2)(h h' - r_1)}{r_1 h (1 + h'^2)^{3/2}}$$

Using the equation of state (14), the equations of motion in the fluid interior

$$\frac{\partial \rho}{\partial v_1} = 3(\rho - \rho_0) \frac{2v_1}{1 - v_1^2 - v_2^2} \quad \frac{\partial \rho}{\partial v_2} = 3(\rho - \rho_0) \frac{2v_2}{1 - v_1^2 - v_2^2}$$

are easily solved and we find

$$(\rho - \rho_0)(1 - v_1^2 - v_2^2)^3 = 5K\rho_0 \quad P = \rho_0 \left(\frac{K}{(1 - v_1^2 - v_2^2)^3} - 1 \right) \quad \mathcal{T} = \gamma \left[\frac{K\rho_0}{\alpha} \right]^{1/6}.$$

Integrating the equations of motion (77) across the surface we obtain the condition (the upper sign should be used for upper surfaces)

$$\frac{K}{(1 - \omega_1^2 r_1^2 - \omega_2^2 h^2)^3} - 1 = \mp \frac{\sigma}{\rho_0} \frac{r_1 h h'' + (1 + h'^2)(h h' - r_1)}{r_1 h (1 + h'^2)^{3/2}} \quad (78)$$

Unfortunately we have not yet been able to solve this equation; we postpone further analysis of (78) to future work. In the rest of this appendix we qualitatively describe possible types of solutions to these equations, and their bulk dual horizon topologies.

In fig.18, we have sketched some possible topologies for these solutions. The first touches both the $r_1 = 0$ and $r_2 = 0$ axes and we refer to this as a ball. The second type only touches one of these axes and we refer to this as a ring. The third type touches neither of the axes, as the plasma has the topology of a solid three-torus we refer to this as a torus.

Each of these could be pinched near either axis, and there could be hollow versions (though the considerations of §6 make it seem unlikely that hollow configurations will actually be solutions).

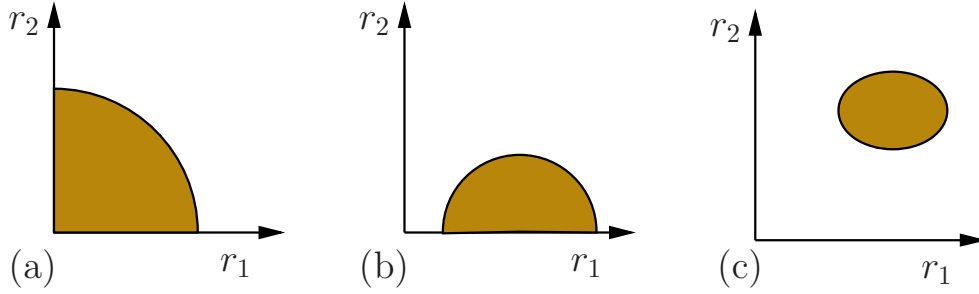


Figure 18: Topologies of five dimensional solutions.

The horizon topology of the dual black object can be found by fibering three circles over the shapes in fig.18. One of these circles degenerates at each axis (the angular coordinates ϕ_1 and ϕ_2), and the other degenerates on the fluid surface (the Scherk-Schwarz circle). The topologies generated are:

Horizon topology	Plasma topology	Object
S^5	B^4	Ball
$S^4 \times S^1$	$B^3 \times S^1$	Ring
$S^3 \times S^1 \times S^1$	$B^2 \times S^1 \times S^1$	Torus
$S^3 \times S^2$	$B^1 \times S^3$	Hollow ball
$S^2 \times S^2 \times S^1$	$B^1 \times S^2 \times S^1$	Hollow ring
$S^2 \times S^1 \times S^1 \times S^1$	$B^1 \times S^1 \times S^1 \times S^1$	Hollow Torus
$S^1 \times S^1 \times S^1 \times S^1 \times S^1$	None	None

B Notation

We work in the $(-++)$ signature. μ, ν denote space-time indices.

Symbol	Definition	Symbol	Definition
\mathcal{F}	Plasma free energy	f	Free energy density
\mathcal{E}	Plasma energy	ρ	Proper density
\mathcal{S}	Plasma entropy	s	Proper entropy density
\mathcal{T}	Plasma temperature	P	Pressure
ρ_0	Plasma vacuum energy	\mathcal{T}_c	Deconfinement temperature
α	see (12)	ρ_c	Deconfinement density
$T^{\mu\nu}$	Stress tensor	u^μ	$\frac{dx^\mu}{d\tau} = \gamma(1, \vec{v})$
σ	Surface tension	γ	$(1 - v^2)^{-1/2}$
$f(x)$	Surface at $f(x) = 0$	ω	Angular velocity
f_μ	$\partial_\mu f / \sqrt{\partial f \cdot \partial f}$	v	ωr
$\theta, \sigma^{\mu\nu}, a^\mu, P^{\mu\nu}$	see (7)	ζ, η	Bulk, shear viscosity
q^μ	Heat flux	κ	Thermal conductivity

Symbol	Definition	Symbol	Definition
$\tilde{\omega}$	$\sigma\omega/\rho_0$	\tilde{r}	$\rho_0 r/\sigma$
r_o	Outer radius	v_o	ωr_o
r_i	Inner radius	v_i	ωr_i
\tilde{r}_o	$v_o/\tilde{\omega}$	$g_{\pm}(v)$	Boundary conditions (36)
\tilde{r}_i	$v_i/\tilde{\omega}$		
E	Ball/ring energy	S	Ball/ring entropy
L	Angular momentum	T	Ball/ring temperature
Ω	Ball/ring angular velocity	Δu	Validity criterion (54)
$\tilde{E}, \tilde{L}, \tilde{S}, \tilde{T}, \tilde{\Omega}$	See (41)	β	$(\partial\tilde{S}/\partial\tilde{E})_{\tilde{L}}$
O,A,B,C	Existence regions, see fig.5	ψ	$(\partial\tilde{S}/\partial\tilde{L})_{\tilde{E}}$
$\hat{O}, \hat{A}, \hat{B}, \hat{C}$	Existence regions, see fig.7	x, y	Boundary scalings in §§5.4
h	Surface height $z = h(r)$	\tilde{h}	$\tilde{\omega}h$
H	Mean curvature	K, C, D	Integration constants in §6
$\Delta\tilde{h}, Q$	Consistency conditions (73,74)	G	Curvature in §A

References

- [1] E. Witten, “Anti-de Sitter space, thermal phase transition, and confinement in gauge theories,” *Adv. Theor. Math. Phys.* **2** (1998) 505–532, [hep-th/9803131](#).
- [2] O. Aharony, S. Minwalla, and T. Wiseman, “Plasma-balls in large N gauge theories and localized black holes,” *Class. Quant. Grav.* **23** (2006) 2171–2210, [hep-th/0507219](#).
- [3] D. T. Son and A. O. Starinets, “Viscosity, Black Holes, and Quantum Field Theory,” [arXiv:0704.0240 \[hep-th\]](#).
- [4] V. Cardoso and O. J. C. Dias, “Rayleigh-Plateau and Gregory-Laflamme instabilities of black strings,” *Phys. Rev. Lett.* **96** (2006) 181601, [hep-th/0602017](#).
- [5] V. Cardoso, O. J. C. Dias, and L. Gualtieri, “The return of the membrane paradigm? Black holes and strings in the water tap,” [arXiv:0705.2777 \[hep-th\]](#).
- [6] V. Cardoso and L. Gualtieri, “Equilibrium configurations of fluids and their stability in higher dimensions,” *Class. Quant. Grav.* **23** (2006) 7151–7198, [hep-th/0610004](#).
- [7] C. W. Misner, K. S. Thorne, and J. A. Wheeler, *Gravitation*. W. H. Freeman and company, San Francisco, 1973.
- [8] R. Emparan and H. S. Reall, “A rotating black ring in five dimensions,” *Phys. Rev. Lett.* **88** (2002) 101101, [hep-th/0110260](#).
- [9] R. Emparan and H. S. Reall, “Black rings,” *Class. Quant. Grav.* **23** (2006) R169, [hep-th/0608012](#).

- [10] H. Elvang, R. Emparan, and A. Virmani, “Dynamics and stability of black rings,” *JHEP* **12** (2006) 074, [hep-th/0608076](#).
- [11] R. Emparan, “Rotating circular strings, and infinite non-uniqueness of black rings,” *JHEP* **03** (2004) 064, [hep-th/0402149](#).
- [12] H. Poincare, “Sur l’équilibre d’une masse fluide animée d’un mouvement de rotation,” *Acta Mathematica* **7** (1885) 259–380.
- [13] G. Arcioni and E. Lozano-Tellechea, “Stability and critical phenomena of black holes and black rings,” *Phys. Rev.* **D72** (2005) 104021, [hep-th/0412118](#).
- [14] J. Katz, “On the number of unstable modes of an equilibrium,” *Monthly Notices of the Royal Astronomical Society* **183** (June, 1978) 765–770.
- [15] J. Katz, “On the Number of Unstable Modes of an Equilibrium - Part Two,” *Monthly Notices of the Royal Astronomical Society* **189** (Dec., 1979) 817.
- [16] R. Sorkin, “A Criterion for the onset of instability at a turning point,” *Astrophys. J.* **249** (1981) 254–257.
- [17] R. D. Sorkin, “A Stability criterion for many parameter equilibrium families,” *Astrophys. J.* **257** (1982) 847–854.
- [18] D. Astefanesei and E. Radu, “Quasilocal formalism and black ring thermodynamics,” *Phys. Rev.* **D73** (2006) 044014, [hep-th/0509144](#).
- [19] G. Arcioni and E. Lozano-Tellechea, “Stability and thermodynamics of black rings,” [hep-th/0502121](#).
- [20] E. W. Weisstein, “Surface of Revolution.” From MathWorld—A Wolfram Web Resource. <http://mathworld.wolfram.com/SurfaceofRevolution.html>, 1999.
- [21] R. Emparan and R. C. Myers, “Instability of ultra-spinning black holes,” *JHEP* **09** (2003) 025, [hep-th/0308056](#).
- [22] G. J. Galloway and R. Schoen, “A generalization of Hawking’s black hole topology theorem to higher dimensions,” *Commun. Math. Phys.* **266** (2006) 571–576, [gr-qc/0509107](#).
- [23] K. S. Thorne, D. A. MacDonald, and R. H. Price, *Black Holes: The Membrane Paradigm*. Yale University Press, 1986.
- [24] M. Parikh and F. Wilczek, “An action for black hole membranes,” *Phys. Rev.* **D58** (1998) 064011, [gr-qc/9712077](#).